

Recent Advances toward the Rational Design of Efficient Bifunctional Air Electrodes for Rechargeable Zn–Air Batteries

Fan-Lu Meng, Kai-Hua Liu, Yan Zhang, Miao-Miao Shi, Xin-Bo Zhang, Jun-Min Yan,* and Qing Jiang

Large-scale application of renewable energy and rapid development of electric vehicles have brought unprecedented demand for advanced energy-storage/conversion technologies and equipment. Rechargeable zinc (Zn)–air batteries represent one of the most promising candidates because of their high energy density, safety, environmental friendliness, and low cost. The air electrode plays a key role in managing the many complex physical and chemical processes occurring on it to achieve high performance of Zn–air batteries. Herein, recent advances of air electrodes from bifunctional catalysts to architectures are summarized, and their advantages and disadvantages are discussed to underline the importance of progress in the evolution of bifunctional air electrodes. Finally, some challenges and the direction of future research are provided for the optimized design of bifunctional air electrodes to achieve high performance of rechargeable Zn–air batteries.

1. Introduction

The ever rising energy demand toward future global economy and tremendous risk of climatic degeneration caused by the use of traditional irreplaceable fossil fuels are two major problems for human sustainable development.^[1,2] Therefore, accelerated developing of environment friendly, inexpensive, and sustainable clean energy and reducing pollution are crucial for sustainable development and have been widely concerned around the world. Sustainable energy sources, such as hybrid wind/photovoltaic power system, and technologies to capture and store carbon emissions actuated by them are referred. However, the feature of intermittence and local limitation of these renewable energy make them difficult to merge with the electricity grid.^[3,4] Some advanced energy storage and conversion systems based on electrochemical technologies, such as, secondary batteries, supercapacitors, and fuel cells provide a promising solution for efficient use of renewable electricity.^[5] As always, lithium-ion

batteries are currently the most successful energy storage solutions, but, their high cost and concerns regarding both their safety and the supply of lithium, and insufficient energy density have held back the large-scale applications.^[6,7] With this in mind, alternative inexpensive and electrically rechargeable battery technologies have aroused growing interest.

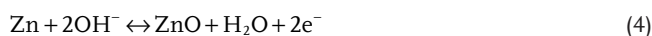
Rechargeable metal–air batteries are attracting more and more attention in the reason of their unique features including greatly high energy density, low cost, and eco-friendly operation.^[8,9] Especially, due to the inexpensive and more abundant in the earth's crust of Zn resource, high relatively high specific energy (1370 W h kg⁻¹), and a volumetric energy

density (1480–9780 W h L⁻¹), Zn–air batteries are by far one of the best options.^[10–12] Besides, the long platform of discharge, high safety of aqueous electrolyte, and longevity make them more meaningful. The structure of a typical Zn–air battery is schematically shown in **Figure 1**, which consists of four major parts, including a Zn metal negative electrode, an alkaline electrolyte, a separator, and a porous air positive electrode. The generation and storage of electricity in rechargeable Zn–air battery systems are realized through redox reactions between positive and negative anodes based on fundamental electrochemical reactions following oxidation and reduction of Zn electrodes, oxygen reduction reaction (ORR), and oxygen evolution reaction (OER) at air electrodes, respectively, corresponding to the discharge and charge processes.

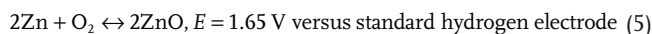
Reactions on the air electrode




Reactions on Zn electrode



Overall reaction:



F.-L. Meng, K.-H. Liu, Y. Zhang, M.-M. Shi, Prof. X.-B. Zhang, Prof. J.-M. Yan, Prof. Q. Jiang
Key Laboratory of Automobile Materials
Ministry of Education and Department of Materials Science and Engineering
Jilin University
Changchun 130012, Jilin, China
E-mail: junminyan@jlu.edu.cn

 The ORCID identification number(s) for the author(s) of this article can be found under <https://doi.org/10.1002/sml.201703843>.

DOI: 10.1002/sml.201703843

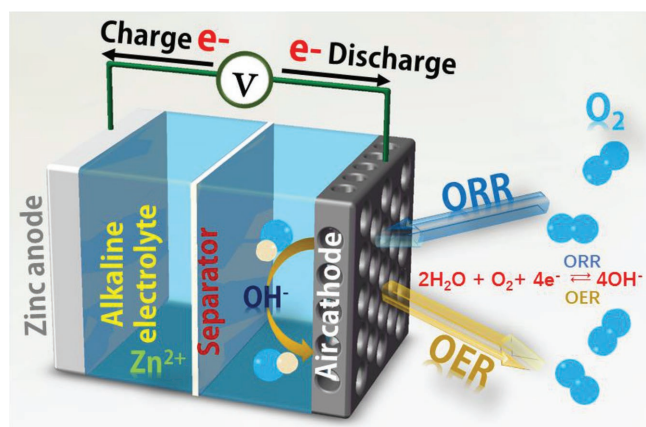


Figure 1. A schematic illustration of an aqueous rechargeable Zn–air battery.

Thermodynamically, both the reactions are spontaneous and produce a theoretical voltage of 1.65 V. However, the redox reactions of oxygen during the charging and discharging cycles are kinetically slow; thus, electrocatalysts are often used to accelerate the process.^[13] Otherwise, some main physical and chemical processes including mass transfer, flow distribution, oxygen storage, and catalyst deactivation are also important, which are generally influenced by the structure of air electrodes. Therefore, to guarantee the energy and power density, recycling, and other key performance for rechargeable Zn–air batteries, the development of optimized air electrodes with reasonable design and composed of low-cost and earth-abundant elements is very important, which has nowadays attracted much more research interests.

In view of the rapid development of rechargeable Zn–air batteries and the key role of air electrodes, a comprehensive review may provide guidance for further studies and command much more attention to optimized design of efficient bifunctional air electrodes. Herein, we summarize recent progress and significant research in air electrodes for rechargeable Zn–air batteries. Fundamental oxygen electrochemical reactions and configuration of air electrodes are briefly covered first. Then, recent reported typical nonprecious metal–based ORR/OER bifunctional catalysts are summarized briefly and systematically. The following focus is on the newly developed integrated air electrodes. Finally, some current challenges and outlook are discussed. In general, this review underlines the importance for researchers to keep pace with the continuing evolution of bifunctional air electrodes for the rational design from catalysts to architectures to achieve high performance rechargeable Zn–air batteries.

2. Architecture and Reactions of the Air Electrode

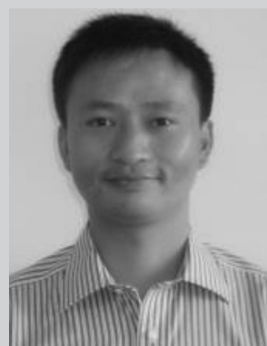
2.1. Oxygen Electrochemical Reactions

The electrochemical reactions of oxygen go through rather slow kinetics, electrocatalysts are generally applied to accelerate both the ORR and OER processes. The reaction process is very complicated and involves a series of complex intermediate reactions



Fan-Lu Meng received his B.S. degree in materials science and engineering from the Jilin University in 2012. He obtained his Ph.D. degree in Materials Science at the Jilin University of China and Inorganic Chemistry at the Changchun Institute of Applied Chemistry, Chinese Academy of Sciences, under the supervision of Prof. Junmin Yan and Prof. Xin-Bo Zhang in 2017. His current interests

include the synthesis and characterization of nanostructures for clean energy conversion reactions.



Xin-Bo Zhang is a Full Professor at the Changchun Institute of Applied Chemistry (CIAC), Chinese Academy of Sciences (CAS). He obtained his Ph.D. in inorganic chemistry from the CIAC. From 2005 to 2009, he worked as a Japan Society for the Promotion of Science (JSPS) postdoctoral fellow (2005–2007) and a New Energy and

Industrial Technology Development Organization (NEDO) research associate (2007–2009) at the National Institute of Advanced Industrial Science and Technology (AIST), Japan. His interests mainly focus on functional inorganic materials for batteries, fuel cells, electrochemical water splitting, and carbon dioxide reduction.



Jun-Min Yan received her Ph.D. degree in inorganic chemistry from the Changchun Institute of Applied Chemistry, Chinese Academy of Sciences in 2006. After that, she worked as a JSPS and NEDO fellow at the National Institute of Advanced Industrial Science and Technology, Japan. At the beginning of 2010, she joined the Department of Materials

Science and Engineering of the Jilin University as a professor of “New Century Excellent Talents in Universities of Ministry of Education of China.” Her current research interests focus on the development of new functional materials for (renewable) energy storage and conversion applications.

along with multistep electron-transfer processes, different reaction mechanisms may take place in different catalysts. During the whole ORR process in the air electrode, oxygen first diffuse

to the catalyst surface from the atmosphere and then adsorbs on it, the oxygen bond is subsequently weakened and broken by electrons transferred from the anode, finally the hydroxyl ion product is released from the catalyst surface into electrolyte.^[14,15] The reduction of oxygen in aqueous electrolytes may take place by two overall pathways separately: a direct four-electron pathway and a two-electron pathway.



For practical battery applications, catalysts that can facilitate ORR through the direct four-electron reduction pathway are highly preferred.

The OER happens as a charging process in reversible Zn–air batteries, involves the reverse process of the ORR, the reaction pathways involved are also rather complex and very different from ORR. For example, the most popular Pt-based catalysts with the highest ORR activity are almost inert when applied as OER electrodes, and suffer from deactivation during operation with severely reduced cycle life. Developing active and durable catalysts for OER, meanwhile, reducing and/or replacing the usage of precious metals with alternatives is the focus of attention over the last decade, and a lot of investigations have been explored. Up to now, most of the proposed possible mechanisms involve that oxygen is usually evolved from the surface of an oxide phase, rather than a pure metal, the electrode materials and site geometry of the metal cations are also probably to change the catalytic process.^[16–19] The multivalence characteristics of transition-metal ions are significant for OER. Because, it is the strong interaction between the metal ions and oxygen intermediates that triggers the reaction. Thereby, the reaction process is influenced by the metal cation site geometry, in this regard, both the adsorption energy of oxygen species and activation energy of cation oxidation state as well as the related coordination number can be changed.^[20,21] In alkaline electrolytes, the mechanism involves the following steps (M is defined as the metal active sites), including the formation of the MOOH intermediate, which subsequently decomposes to O₂, or the direct combination of 2MO to produce O₂.^[18]



2.2. Configuration of the Air Electrode

Currently, most of the electrically rechargeable Zn–air batteries are assembled using a bifunctional air electrode which can simultaneously catalyze ORR and OER. The air electrodes

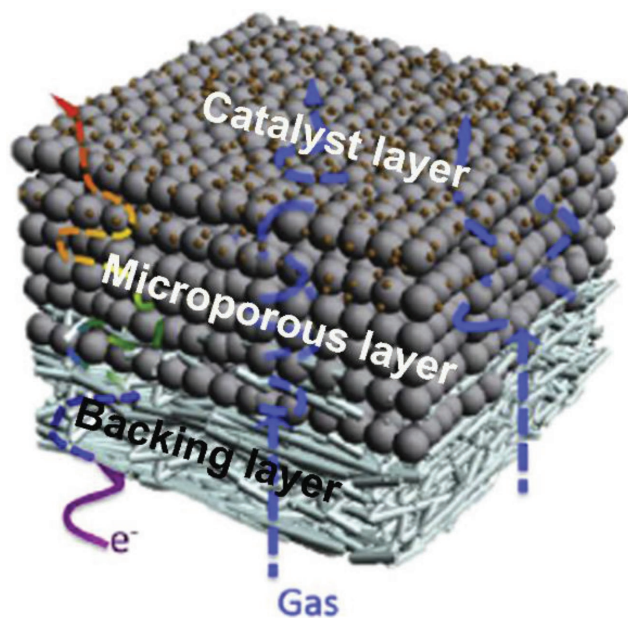


Figure 2. A schematic illustration of a GDL electrode. Reproduced with permission.^[23] Copyright 2017, Elsevier.

are commonly built on a gas-diffusion layer (GDL), similar to that of fuel cells (Figure 2), which plays an important role in turning the performance of bifunctional catalysts on air electrodes. Generally, the GDL first acts as a physical support for the catalyst layer and a collector to possess high electrical conductivity to provide an electrically conductive pathway for current collection. But, more importantly, the GDL should not only promote a uniform and sufficient contact between the air and the catalysts, but also provide a barrier to prevent electrolyte penetration,^[21] so that, hydrophilic and hydrophobic microchannels should be assembled in the same GDL to form interpenetrating subsystems, wherein, the hydrophilic microchannels are designed to allow the immersion of liquid electrolyte, oppositely, the hydrophobic parts play a role of a barrier to block electrolyte from leaking out, and to promote the rapid diffusion of oxygen to the catalytic sites, in which, an optimal gas–electrolyte–catalyst three-phase interface is created. The hydrophilic microchannels are usually composed of catalysts and active carbon.^[22,23] To realize the hydrophobic property, hydrophobic agents such as polytetrafluoroethylene (PTFE),^[24] polyvinylidene Fluoride (PVDF),^[25] and fluorinated ethylene propylene (FEP)^[26] are adopted. These bifunctional air electrodes are highly susceptible to carbon corrosion under high oxidative potential under OER conditions, consequently leading to losses of active surface area, uniform distribution of current, and even severe leakage of electrolyte. Besides, the carbon oxidation generally produces carbon dioxide (CO₂), which can easily react with alkaline electrolytes to form carbonates. Previous results have proved that carbonates not only reduce the electrolyte conductivity, but also clogs pores and decreases the active surfaces in the air electrode when crystallization of carbonates occurs. To circumvent the deactivation problems upon exposure to OER potential regimes, some solutions are proposed. One is to prevent the corrosion of the GDLs either

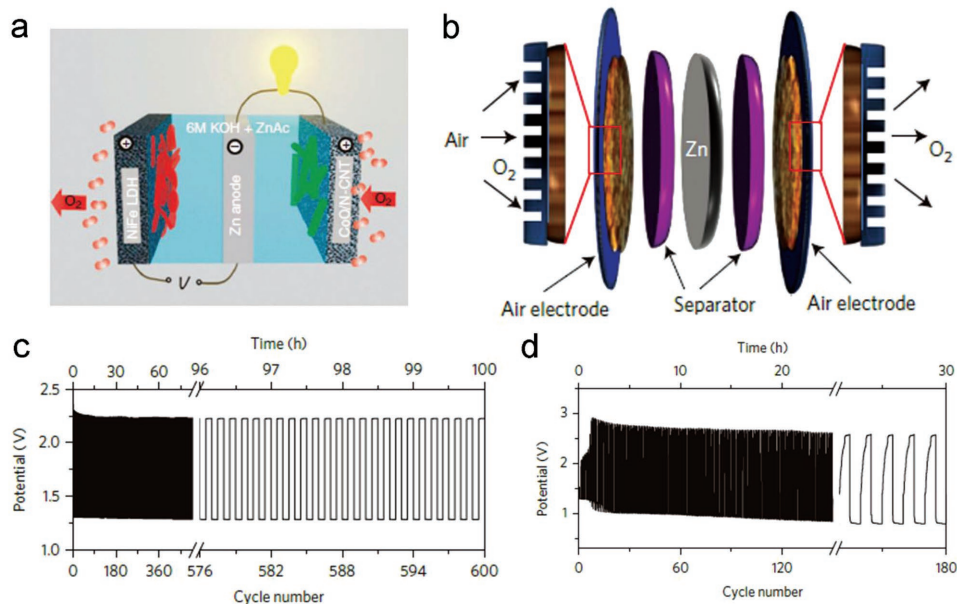


Figure 3. a) Schematic of the three-electrode configuration. Reproduced with permission.^[30] Copyright 2013, Springer Nature. b) Schematic of the basic configuration of a three-electrode Zn–air battery with a structure of button type and c) cycling curves. d) discharge/charge cycling curves for a two-electrode rechargeable Zn–air battery using NPMC-1000 as bifunctional catalyst. Reproduced with permission.^[29] Copyright 2015, Springer Nature.

using graphitized carbon materials with high anticorrosion capacity, or metallic substrates.^[27,28] The other is to explore rechargeable Zn–air batteries in a trielectrode configuration (air/Zn/air).^[29,30] As shown in **Figure 3a**, in a three-electrode configuration, the ORR and OER electrodes are decoupled. During charging process, the OER electrode connected to the Zn anode works, the ORR electrode avoids suffering from positive oxidation potentials. For example, Zhang et al.^[29] proved that the battery performance of their developed 3D N and P-codoped mesoporous nanocarbon (NPMC) foams could be significantly strengthened in an optimized three-electrode configuration (**Figure 3b**), in the circumstances, the ORR activity and OER activity would be regulated independently on each of the two air electrodes to realize a balanced reversibility between oxygen reduction and evolution. Compared to the two-electrode design, the charging–discharging cycles for the three-electrode batteries presented much lower overpotential and better stability (**Figure 3c,d**). In spite of this, multiple electrodes and correlations between them are inevitably to add complexity and cost in the battery assembly, the carbon corrosion of GDLs on the charging air electrode is also unavoidable.

3. Bifunctional Catalysts

In order to accelerate both the ORR and OER process for practical use of rechargeable Zn–air batteries, bifunctional catalysts are very necessary. Until now, many single functional ORR or OER catalysts have been developed with very efficient performance. Although, one of each of these catalysts can be composited and filled in one rechargeable air electrode, other problems come along, such as the accessorial synthesis of materials, increasing cost concerns, and induced manufacturing complexities. In addition, it still faces enormous challenges to find a

stable catalyst material without significantly sacrificing bifunctional catalytic efficiency, mainly in the reason of the wide operating range of the ORR/OER potential during the discharge and charge process,^[31] so that, for the purpose of achieving catalytic efficiency for both the ORR and OER at the same air electrode, exploring ideal ORR/OER bifunctional catalysts is urgent and a lot of efforts have been devoted.^[32–36] In this aspect, various electrocatalysts, such as heteroatom-doped nanostructured carbonaceous materials, metal nanoparticles encapsulated in carbon layer, metal oxides, metal chalcogenides, and their nanocarbon hybrid materials, etc. have been applied in the Zn–air battery system, followed with success of varying degrees.

3.1. Heteroatom-Doped Carbon Materials

Carbon nanomaterials have been adapted as very promising catalysts with high activity and good stability, in addition, the catalytic properties of them could be further improved by the molecular and/or nanoarchitecture engineering under various novel strategies containing heteroatom doping (N, P, S, B, and so on), geometry optimization, and surface functionalization.^[37–44] Significantly, heteroatom doping can greatly boost the ORR activity leading to a favorable formation of OH[−] via the four-electron pathway, in particular, various N-doped carbon materials. Carbon nanomaterials are usually used as ORR catalysts, the bifunctional property is rarely reported, mainly because of their fairly low OER catalytic activity and the unavoidable carbon corrosion under the high oxidation potentials of the OER, which could cause catalyst agglomeration, and block the active surface with formed carbonates to furniture the deactivation of the catalysts.^[18,21] Benefiting from the extensively conjugated structure, graphitic carbon nanomaterials such as carbon nanotubes (CNTs) and graphene naturally

have relatively high oxidation stability, when introducing heteroatom dopants, they could display bifunctional activity and selectivity, as well as the improvement of the overall stability. For example, Xia et al.^[44] reported a hollow framework of nitrogen-doped carbon nanotubes derived from zeolitic imidazole framework, in which, the chemical compositions, crystalline nitrogen-doped carbon nanotubes, and robust hollow structure synergistically made it exhibit remarkable electrochemical properties and stability as a bifunctional catalyst, because, their combination provided excellent conductivity and

remarkable corrosion resistance in a harsh operating environment. Combining N with a second heteroatom, such as S or P forming codoped carbon nanomaterials could change the surface electronic states and polarities to further increase bifunctional activity.^[29,45–49] An important part of this strategy is N, S codoping, for instance, Qu et al.^[47] developed N, S-codoped mesoporous carbon nanosheets using S-modified polydopamine as a precursor (Figure 4a). Benefiting from the multiple doping, this material exhibited excellent ORR/OER bifunctional activity and durability, even better than that of transition-metal

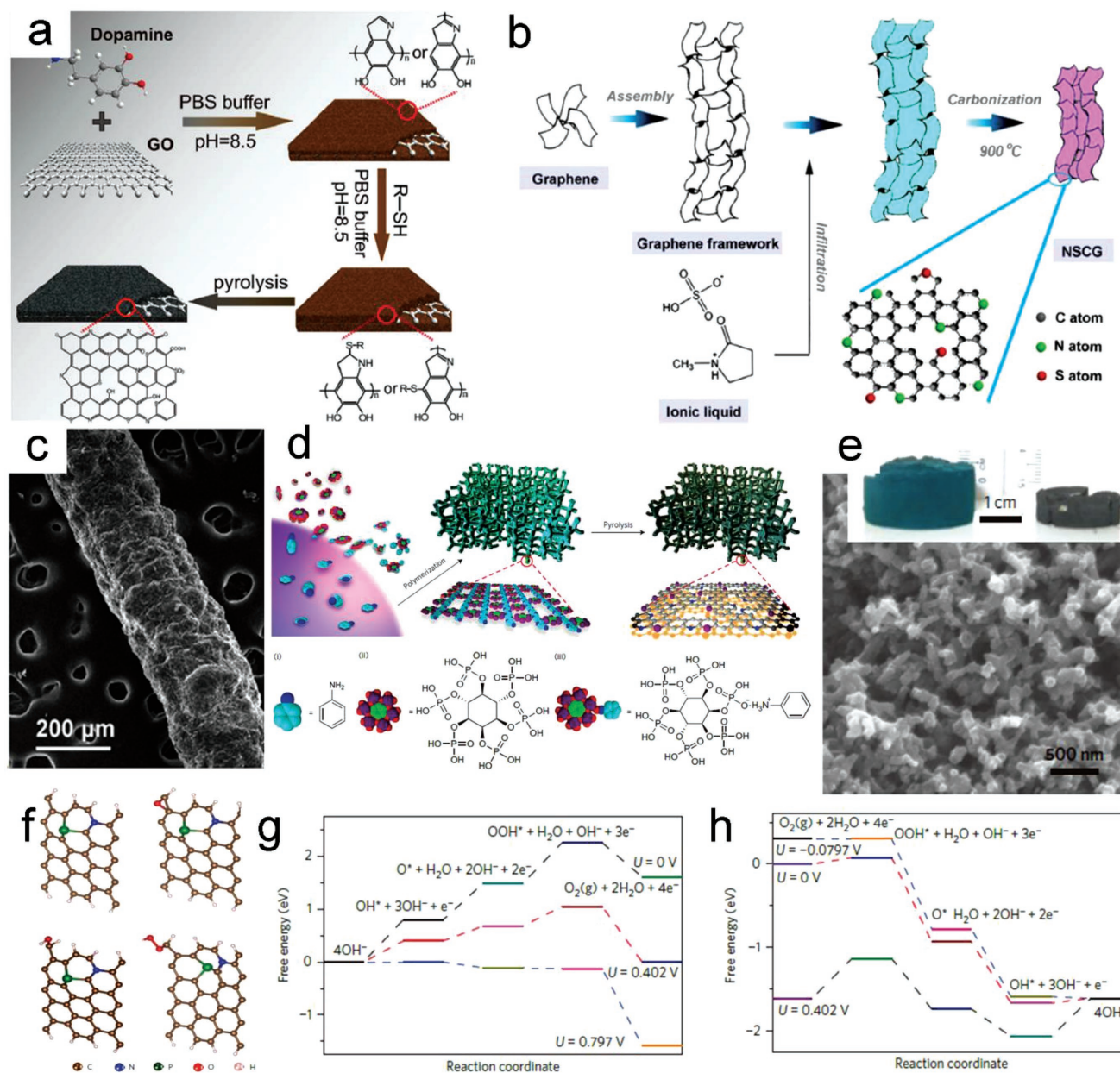


Figure 4. a) Scheme of GDS derived carbon nanosheets (N, S-CNs). Reproduced with permission.^[47] Copyright 2016, Elsevier. b) Synthetic process of N-, S-doped graphene microwires with a small amount of N-, S-doped carbon, and c) the corresponding scanning electron microscopy (SEM) image. Reproduced with permission.^[45] Copyright 2015, Elsevier. d) Schematic diagram of the preparation of NPMC foams, and e) the corresponding SEM image. f) Structures before and after the adsorption of OH^* , O^* , and OOH^* intermediates on N- and P-coupled graphene. g,h) Schematic energy profiles for the OER and ORR pathway. Reproduced with permission.^[29] Copyright 2015, Springer Nature.

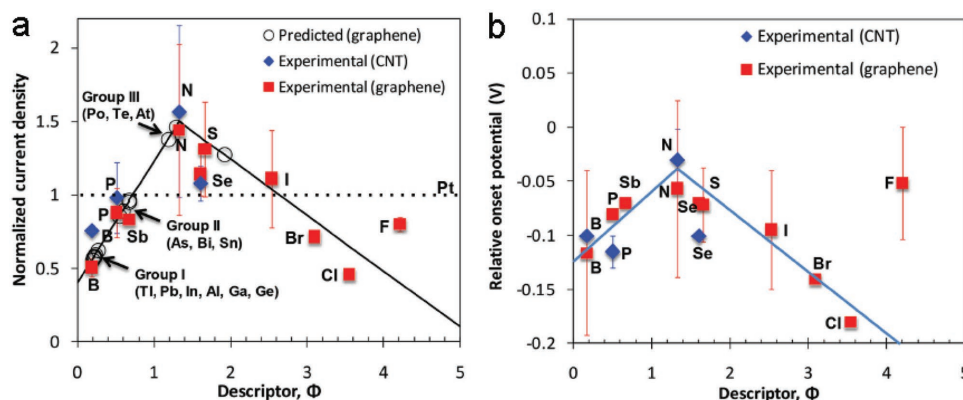


Figure 5. Volcano relationship plots between the descriptor and the intrinsic bifunctional activity of heteroatom-doped carbon-based catalysts. Reproduced with permission.^[50] Copyright 2015, Wiley.

and noble-metal catalysts. Chen et al.^[45] reported a facile path way to fabricate a freestanding N-, S-doped graphene microwire with both high D_{cas} and S_{eff} , of which the key was the use of an ion liquid (*N*-methyl pyrrolidone hydrosulfate) as the heteroatom-rich precursor (Figure 4b,c), in which, the double doping of N and S into graphene could bring a lot of active sites (C–N–S charge spin density 0.43), thus resulting in higher OER catalytic activity. B represents another important doping element, for example, Qian et al.^[38] developed a B–N dual-doped highly porous carbon (BNPC) for ORR and OER catalysis by pyrolyzing a Zn–metal–organic framework (MOF) (MC-BIF-1S), which exhibited high bifunctional catalytic activity. Besides the discussed trielectrode configuration (air/Zn/air), the performance of NPMC^[29] was boosted by efficient P doping and a large surface area of $\approx 1663 \text{ m}^2 \text{ g}^{-1}$ from its preparation of the pyrolysis of a phytic acid-mixed polyaniline aerogel with a one-step scalable process (Figure 4d,e). Density functional theory calculations and first-principle simulations revealed the essentially key roles of graphene edge effects and N, P codoping. That was, the adsorption of chemical species and catalytic activity was determined by the distance of doping sites from the graphene edge, in which, OER and ORR occurred at different sites separately near the edge of the graphene (Figure 4f–h). Understanding the exact catalytic reaction mechanisms of the ORR and OER on heteroatom-doped nanocarbon is thereby of importance to finely tune the bifunctional activity and selectivity, as well as the improvement of the overall stability. Recently, Zhao et al.^[50] explored the relationship between the intrinsic activity and various heteroatoms in carbon-based electrocatalysts, and established a volcano curve to predicate the ORR/OER bifunctional catalytic activities (Figure 5). The combined effects of the electron affinity and the electronegativity of dopants on charge redistribution over the carbon surface were taken into consideration. Such descriptor provides a guide for the design of metal-free p-orbital element-doped carbon-based catalysts with improved ORR/OER bifunctional activities.

3.2. Metal Nanoparticles Encapsulated in Carbon Layers

Recently, hybrid materials with transition metals (TMs) encapsulated in graphitic layers (Figure 6a,b) are found to be as

efficient electrocatalysts to facilitate both ORR and OER, the Fe, Ni, and Co single metal nanoparticles or their combination encapsulated in graphene layers or carbon nanotubes are most special.^[51–56] Transition-metal nanoparticles could serve multiple purposes at the same time to influence the surface carbon layer, including increasing its graphitization degree during carbonization, and transferring electron to it. In turn, the surface carbon layer could prevent oxidation, acid leaching, and aggregation of encapsulated transition-metal nanoparticles in the electrocatalytic process.^[57] The catalytic activity of these catalysts is strongly dependent on two crucial factors, including the intrinsic activity and the density of active sites. The intrinsic activity is determined by the electronic structure of surface graphitic layer, which can be adjusted by an electronic modulation effect from suitable metal cores, wherein, the interaction between them changes the local work function of the shell, inducing surprisingly high chemical activities.^[57,58] Besides, the doping nitrogen in carbon lattice can further induce uneven charge distribution of the adjacent carbon atoms. An extra synergistic effect between the doped nitrogen and the encapsulated transition-metal nanoparticles also stimulates an enhanced electrocatalytic activity (Figure 6c).^[54,56] The density of active sites is deeply based on the effective area of modulated surface carbon, which is mainly a function of metal core size, loading, and dispersion.

Generally, these type of catalysts are crucially dependent on high temperature synthesis. Through reasonable pyrolysis of the metal salts and organic molecular compounds, Wang et al.^[57] reported the synthesis of high-density iron nanoparticles encapsulated within nitrogen-doped carbon nanoshell (Fe@N-C) by solid-phase precursor's pyrolysis of dicyandiamide and ammonium ferric citrate. During carbonization process, high graphitization degree in the carbon phase was generated with the help of a number of iron nanoparticles, which could highly facilitate electrical conductivity in the electrocatalytic process, so, the resulting Fe@N-C-700 material showed excellent bifunctionality for ORR and OER in alkaline medium compared to state-of-the-art commercial Pt/C and IrO₂, and high Zn–air battery performance. Despite realizing high performance, the physical mixing of organic molecular compounds and metal salts frequently fails in controlling the uniform distribution of different components because of their

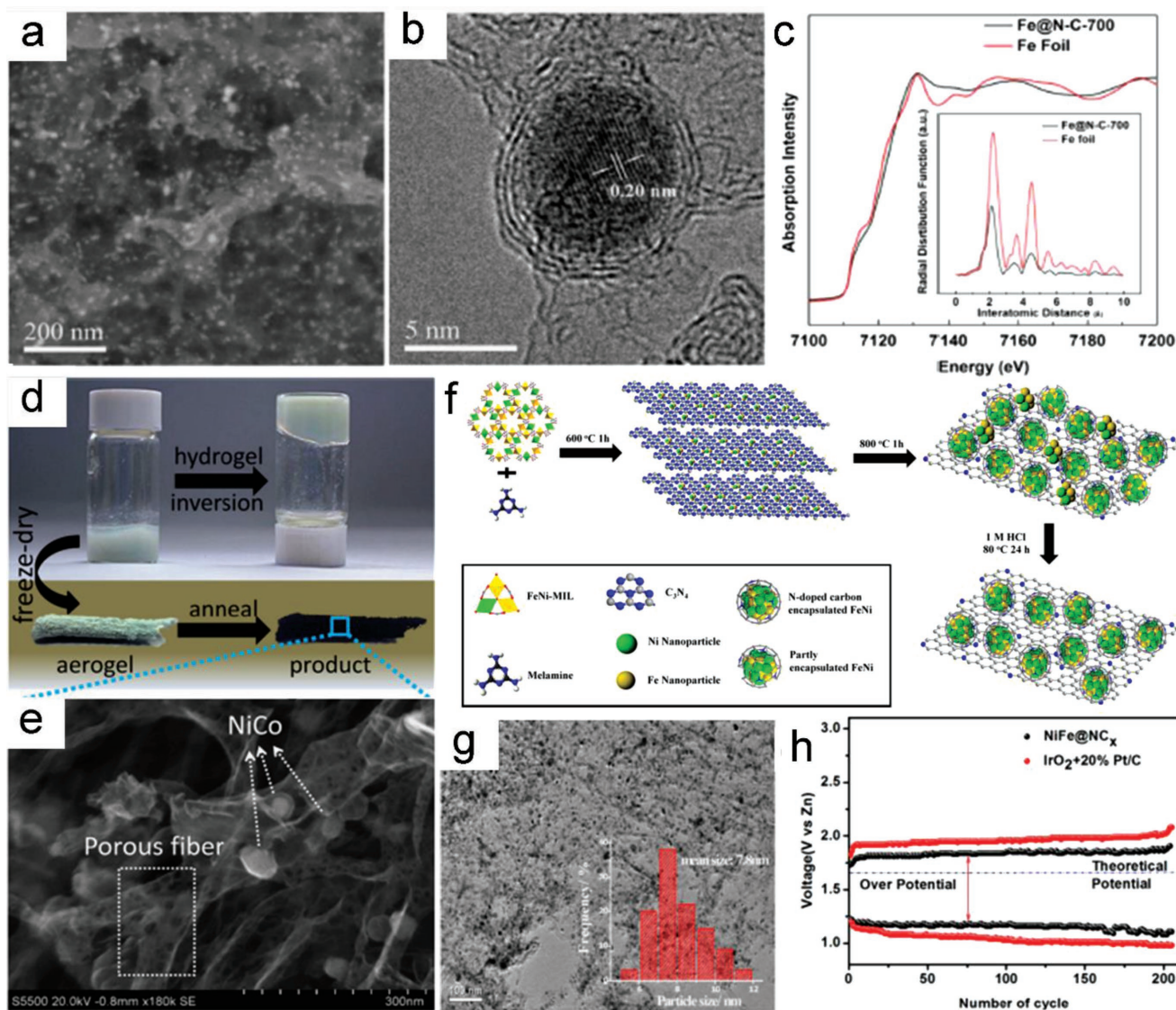


Figure 6. Physicochemical characterization of Fe@N-C-700. a) SEM, b) transmission electron microscopy (TEM), and c) X-ray absorption near edge structure (XANES) and extended X-ray absorption fine structure (EXAFS) spectra. Reproduced with permission.^[57] Copyright 2015, Elsevier. d) Fabrication process and e) the SEM image for the 3D NiCo/porous fibrous carbon (PFC) aerogels. Reproduced with permission.^[61] Copyright 2016, American Chemical Society. f) Schematic illustration of the synthetic strategy and g) TEM image (inset: the corresponding particle-size distribution histogram) of the TMs@NC_x Composite. h) The cycling curves performed at 10 mA cm⁻² with a duration of 600 s per cycle. Reproduced with permission.^[71] Copyright 2016, American Chemical Society.

bad compatibility, which inevitably leads to the agglomeration of the metal particles and the microstructural inhomogeneity, thus hindering its further improvement. Accordingly, better efforts might be required to controllably tune the activity. It is well known that the sol-gel process has the potential advantage that different components could be homogeneously mixed at atom level.^[59,60] For example, based on the sol-gel chemistry, Fu et al.^[61] demonstrated an excellent bifunctional catalyst composed by porous fibrous carbon aerogels and the anchored NiCo nanoparticles (NiCo/porous fibrous carbon (PFC) aerogels), using a novel K₂Ni(CN)₄/K₃Co(CN)₆-chitosan hydrogel system (Figure 6d,e). However, the sol-gel and following pyrolysis most often failed in controlling the pore structures suitably.

In view of the well-defined coordination environment, ordered arrangement in the framework, and periodic porous structure, MOFs can act as perfect encapsulators for metal ions;^[62–64] pyrolysis of MOFs and their compounds is defined as one of the most efficient means to solve this problem, besides, the tailored metal coordination center and organic ligands, their rich porous structure and higher specific surface area provide them more possibilities. A variety of different MOF types with diverse metals and ligands have been developed, Co-, Fe-based ones are the most popular and efficient, such as zeolitic imidazolate frameworks (ZIFs),^[65–67] iron(III)-based metal-organic frameworks (MILs),^[68,69] and so on. As one of the simplest MOFs,^[70] the cobalt analog of Prussian blue can be directly

used to synthesize a metallic cobalt core/graphene shell bifunctional electrocatalyst as a single precursor. Notwithstanding the simple process, the agglomeration of the metal particles is inevitable due to the implicit structural factor of Prussian blue. Recently, Zhu et al.^[71] demonstrated catalysts featured with thin graphene nanosheets coupling with full encapsulated ultrafine and high-loaded (≈ 25 wt%) transition-metal nanoparticles (TMs@NC_x) depending on a unique two stage encapsulation strategy of pyrolysis of MOF-based NiFe-MILs and melamine (Figure 6f,g). Based on the modulation of the electronic structure of outer carbon layers by electron penetration from NiFe cores, increased active site density from size reduced encapsulated nanoalloy, and enhanced electron density in graphene shells, the best NiFe@NC_x catalyst exhibited superb electrocatalytic activity and high stability with an onset potential of 1.03 V for ORR and an overpotential of only 0.23 V at 10 mA cm⁻² for OER. Rechargeable Zn-air battery using NiFe@NC_x catalyst exhibited an unprecedented long-term cycle stability at 10 mA cm⁻² (Figure 6h).

3.3. Transition-Metal Oxides and the Nanocarbon Hybrid Materials

Transition-metal oxides stand for a broad categories of oxygen catalysts with rich, low cost, easy preparation, environmental friendliness, etc.^[72–74] Transition-metal elements have more than one valence, produce various oxides with different crystal structures. Their electrocatalytic activity is associated with the ability of transformation between different valence states of cations, especially when forming redox couples under the oxygen reduction or evolution potentials.^[73] The chemical constitution, oxidation state, texture, morphology, and crystal structure have been adopted as functional adjustment of the electrocatalytic properties.^[21] In light of the published results, some

transitional-metal spinel oxides, including Co₃O₄,^[75] MnO₂,^[76] MnCo₂O₄,^[77] NiCo₂O₄,^[78] etc., are widely applied in Zn-air batteries. Mixed-metal oxides with a perovskite structure represent another important type of ORR/OER bifunctional catalysts.^[79] Rational control of the TM center and TM/A composition allows the ORR/OER catalysis to be tuned on perovskite-type transition-metal oxides. For example, the lanthanum-based ones, such as La-(Co_{0.55}Mn_{0.45})_{0.99}O₃, LaTi_{0.65}Fe_{0.35}O₃, LaMO₃ (M = Fe, Co, Ni, Cr, and Mn),^[80–82] have received a lot of attention as bifunctional electrocatalysts in Zn-air batteries in recent years. Quite recently, chemical combination of different oxides is demonstrated an effective way to achieve high-performance bifunctional electrocatalysts. In this regard, Guo et al.^[83] provided a typical example of CoO/hi-Mn₃O₄ with high-energy interfacial structures by chemical coupling of active CoO nanoclusters and high-index facet Mn₃O₄ nano-octahedrons (hi-Mn₃O₄) to fabricate the bifunctional electrocatalyst (Figure 7b–f). The strong coupling interactions were confirmed throughout a series of characterizations (Figure 7g,h). The closely spaced Mn^{III}-O pair in hi-Mn₃O₄ acted as electron acceptor to draw electrons from CoO, leading to high-energy interfacial Mn-O-Co species and high oxidation state CoO, which featured a large number of active sites, favored fast charge transfer, reversible oxidation capability, and enhanced higher intrinsic catalytic activity than conventional metal oxides. These advantages were finally demonstrated by 1.2 times higher OER activity than that of Ru/C, a competitive ORR activity to that of Pt/C, and a stable cycling performance in its Zn-air battery (Figure 7i).

Although achieving great development of transition-metal oxides, the electrocatalytic performance is still unsatisfactory, which is heavily hampered by some important drawbacks and limitations, including the inherent low conductivity and serious aggregation of nanoparticles. Carbon-based hybrid bifunctional catalyst typically consists of strongly coupled oxide nano-materials and functionalized carbons are then put forward to

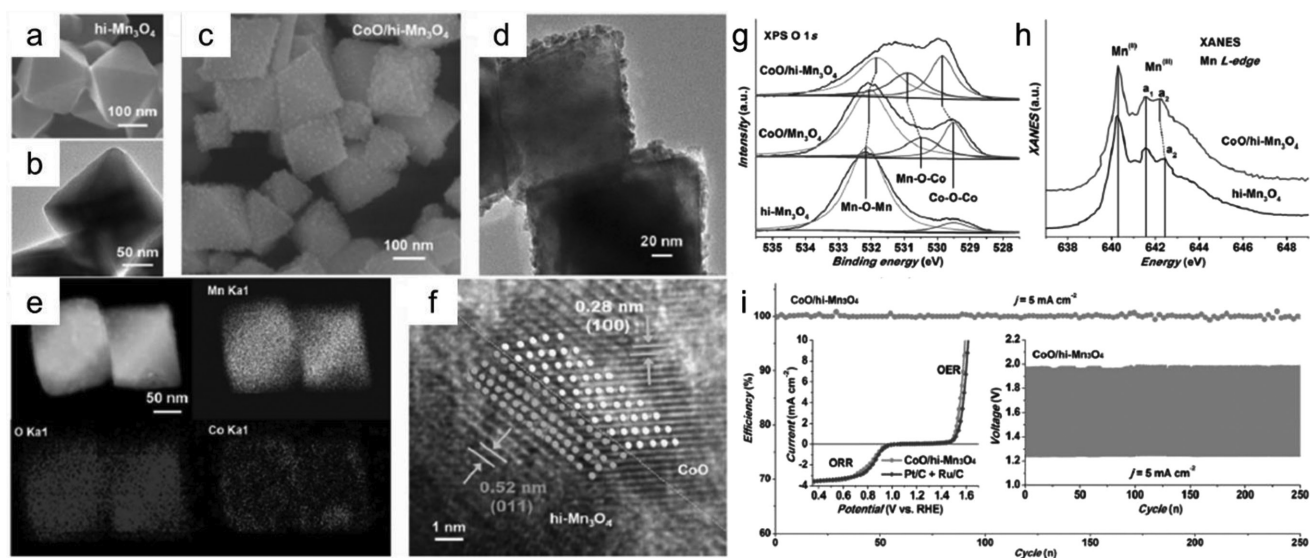


Figure 7. a,b) SEM and TEM images of hi-Mn₃O₄ and c,d) CoO/hi-Mn₃O₄. e) Elemental mapping and f) high-resolution TEM (HRTEM) image of CoO/hi-Mn₃O₄. g) X-ray photoelectron spectroscopy (XPS) O1s spectra and h) synchrotron near edge X-ray absorption finestructure (NEXAFS) Mn L-edge spectra of the materials studied. i) Efficiency against discharging cycles of a Zn-air battery with CoO/hi-Mn₃O₄ air electrode. The insets are polarization curves and galvanostatic cycling profiles at a current density of 5 mA cm⁻². Reproduced with permission.^[83] Copyright 2017, Wiley.

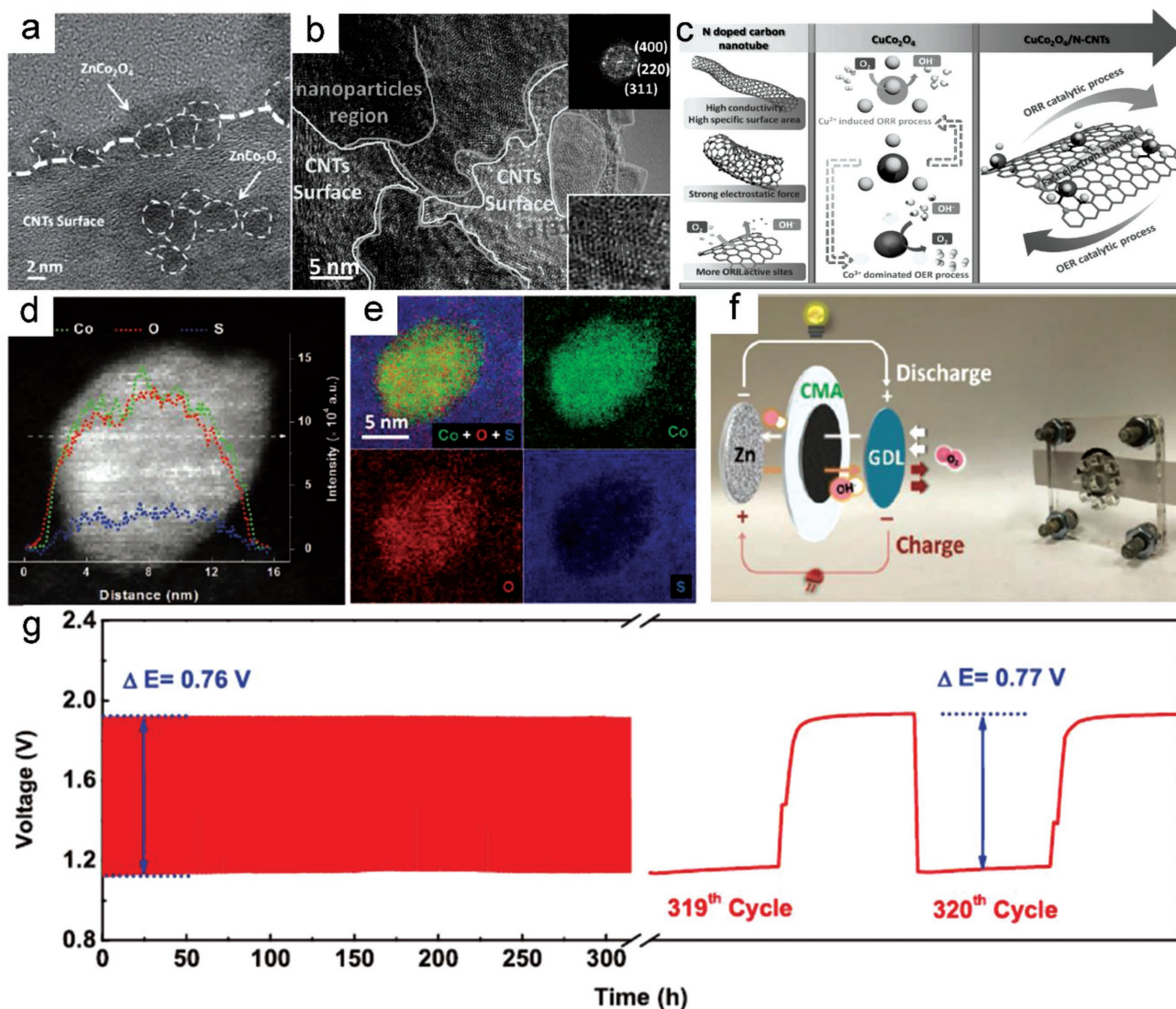


Figure 8. a) High-resolution TEM images of ZnCo_2O_4 quantum dots anchored on N-CNT surface. Reproduced with permission.^[88] Copyright 2016, Wiley. b) TEM and HRTEM images of $\text{CuCo}_2\text{O}_4/\text{N-CNTs}$. c) Illustration of the catalytic process of $\text{CuCo}_2\text{O}_4/\text{N-CNTs}$. Reproduced with permission.^[89] Copyright 2017, Wiley. d,e) Aberration-corrected electron energy loss spectroscopy (EELS) elemental mapping and the corresponding EELS line profile of $\text{Co}_{0.87}\text{S}_{0.13}/\text{GN}$. f,g) Scheme of the quasi-solid-state zinc–air battery configuration and discharge and charge cycling performances. Reproduced with permission.^[90] Copyright 2017, Wiley.

overcome that.^[84–87] For example, by a simple electrospinning technique, Prabu et al.^[81] reported a new bifunctional ORR and OER catalyst, in which, perovskite $\text{LaTi}_{0.65}\text{Fe}_{0.35}\text{O}_{3-\delta}$ (LTFO) nanoparticles were entangled both at the surface and within the nitrogen-doped carbon nanorods (NCNRs). The porous nanorod morphology provided a high surface area and good dispersion of active perovskite centers on the surface to make sure they are easily accessible for electrocatalytic testing over long-term cycling of zinc–air batteries, which shows a modest overpotential and a stable discharge potential region for prolonged periods of at least 12 h. But beyond that, the unexpected synergistic effect between the catalyst and substrate may further generate more excellent catalytic activity. The recognition of the synergistic coupling effect between spinel- Co_3O_4 nanoparticles and N-doped graphene or mildly oxidized CNTs has been proven beneficial for improved bifunctional activity, as

well as stability, compared to that of Co_3O_4 .^[84] To expand this strategy for further improved performance, recent reports have developed a series of efficient catalysts by reducing particle size, adjusting the stoichiometric, introducing doped elements, and/or compositing them. For instance, Liu et al.^[88] synthesized $\text{ZnCo}_2\text{O}_4/\text{N-doped CNT}$ through a controllable nanoscale synthetic strategy, affording ZnCo_2O_4 particles with ultrasmall size— ZnCo_2O_4 quantum dots homogeneously dispersed on N-CNT (Figure 8a). Cheng et al.^[89] further carried forward this strategy (Figure 8b), in which, they uncovered a synergistic effect in the synthesized catalysts of N-doped carbon nanotubes decorated by CuCo_2O_4 as well as the increased catalytic sites caused by Cu doping (i.e., Cu^{2+} and Cu–N) by combining spectroscopic characterization and electrochemical studies (Figure 8c). Different from the metal doping to replace the Co sites, by the composition of sulfur-deficient cobalt oxysulfide

($\text{CoO}_{0.87}\text{S}_{0.13}$) and nitrogen-doped graphene nanomeshes (GN), Fu et al.^[90] reported a hybrid catalyst, which takes full advantage of the defect chemistries including nonstoichiometric, oxygen-vacancy-rich, and edge-nitrogen doping (Figure 8d,e). In addition, the GN helped to promote the intimate electronic contact between $\text{CoO}_{0.87}\text{S}_{0.13}$ nanoparticles and provide adequate open space and short diffusion channels for reactants and intermediates. A remarkable improvement in bifunctional electrocatalytic performance guaranteed the successful application in Zn–air batteries. As a freestanding catalyst, the assembly quasi-solid-state Zn–air batteries achieved a low discharge–charge overpotential of 0.77 V at 20 mA cm⁻² and cycling stability over 300 cycles (Figure 8f,g).

3.4. Transition-Metallic Chalcogenides and the Nanocarbon Hybrid Materials

With the rapid progress of material science, late transition-metal chalcogenides with various combinations of transition metals (Fe, Co, etc.) and chalcogens (S, Se, etc.) have been

demonstrated high electrocatalytic activity toward ORR and/or OER with a high tolerance against small organic molecules.^[91] Among them, cobalt sulfides have drawn many applications in ORR,^[92–94] theoretical calculations have already predicted that Co_9S_8 catalyzed the ORR via a four-electron reaction pathway, similar to Pt surface. Unfortunately, it shows moderate OER capability. To realize a balance between ORR and OER activities to achieve high-performance bifunctional electrocatalysts used in rechargeable Zn–air batteries, various strategies are developed by precise control of nanostructures and components. For example, Cai et al.^[95] developed an oxygen-incorporated amorphous cobalt sulfide porous nanocubes (A- $\text{CoS}_{4.6}\text{O}_{0.6}$ PNCs), that showed advantages over the benchmark catalysts (Figure 9a,b). By simply immersing Co-based hydroxide precursor into solution with high-concentration S^{2-} , Wang et al.^[96] converted transition-metal hydroxides to hydroxysulfides with excellent morphology preservation and the integration of hydroxides and sulfides at an atomic level at room temperature. The synthesized $\text{Co}_3\text{FeS}_{1.5}(\text{OH})_6$ displayed high intrinsic reactivity and electrical conductivity (Figure 9c,d), in which, the electron structure of the active sites was adjusted by anion modulation.

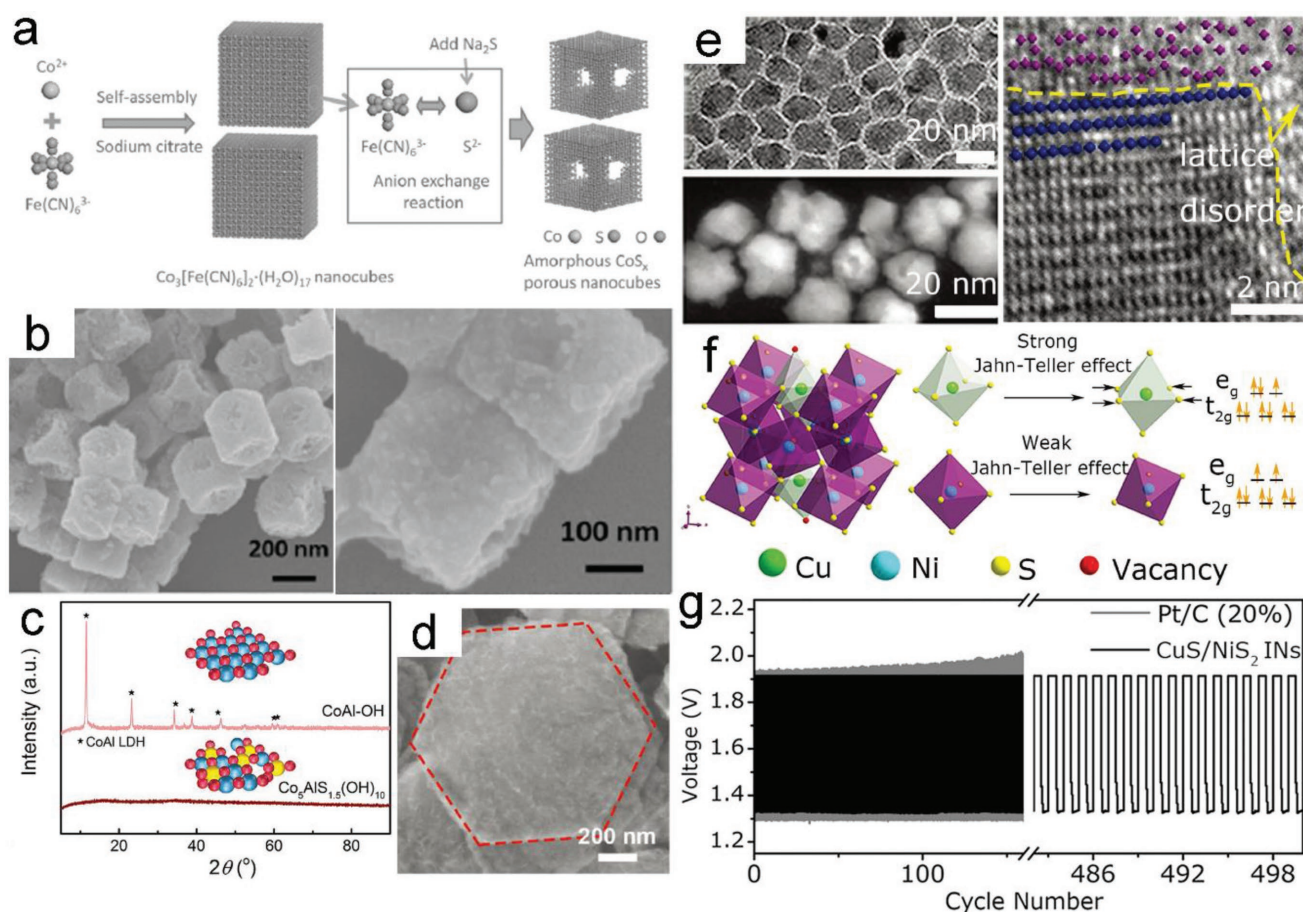


Figure 9. a) Illustration of synthesized process and b) SEM images of A- $\text{CoS}_{4.6}\text{O}_{0.6}$ PNCs. Reproduced with permission.^[95] Copyright 2017, Wiley. c) X-ray diffraction (XRD) spectra and schematic of the metal hydroxides and metal hydroxysulfides of CoAl-OH and $\text{Co}_3\text{AlS}_{1.5}(\text{OH})_{10}$, and d) SEM image of $\text{Co}_3\text{AlS}_{1.5}(\text{OH})_{10}$. Reproduced with permission.^[96] Copyright 2017, Wiley. e) TEM, HRTEM, and high angle annular dark field image-scanning transmission electron microscopy (HAADF-STEM) images of CuS/NiS₂ INs. f) Schematic illustration of the locations of S vacancies in CuS/NiS₂ INs and Jahn–Teller effect for the subtle distortion in CuS/NiS₂ INs lattice. g) Galvanostatic discharge–charge cycling curves at 25 mA cm⁻² of the Zn–air batteries with CuS/NiS₂ INs as the catalyst. Reproduced with permission.^[97] Copyright 2017, Wiley.

Besides, structural advantages including nanosized particles, an amorphous surface, and numerous electron pathways provided the full exposure of active sites and benefitted electron transfer, thus, leading to efficient bifunctional electrocatalytic activity for ORR/OER used in Zn–air batteries. Recently, An et al.^[97] reported a class of CuS/NiS₂ interface nanocrystal (IN) catalysts with atomic level–coupled nanointerface, subtle lattice distortion, and plentiful vacancy defects (Figure 9e), wherein, the lattice distortion in CuS/NiS₂ was caused by the strong Jahn–Teller effect of Cu (Figure 9f), the strong atomic level–coupled interface of CuS and NiS₂ domains, and distinct vacancy defects could provide numerous effective active sites for their excellent bifunctional performance, which made the assembled Zn–air batteries display a large peak power density (172.4 mW cm⁻²), a high specific capacity (775 mAh g_{Zn}⁻¹), and long cycle life (up to 83 h) (Figure 9g).

To further compensate the poor electrical conductivity, the combination of active species and carbonaceous nanomaterials

(e.g., CNT and graphene) has been proven to be a promising strategy to achieve the resultant hybrids with excellent electrocatalytic activity and satisfied stability by virtue of improved overall conductivity and the coupling synergetic effect.^[98–100] Furthermore, doping heteroatoms (N, S, P) into the carbon framework could further optimize the surface electronic structure configurations and the adsorption/desorption behaviors toward oxygen intermediates, thus facilitating the electrocatalytic kinetic processes in metal–air chemistries. Recently, our group for the first time in situ anchored Co₉S₈ NPs on N, S-codoped porous carbon tubes (Co₉S₈/NSPC) as a bifunctional ORR/OER electrocatalyst with the help of a water-soluble Na₂SO₄ nanowire template and an all-in-one N, S, and C precursor of poly(2-aminothiazole) (P-2AT) (Figure 10a). The intimate contact between Co₉S₈ and NSPC brought a cooperative effect, which was also confirmed by density functional theory (DFT) calculations (Figure 10b).^[98] Compared to monometallic sulfides, the synergistic effect of different transition-metal

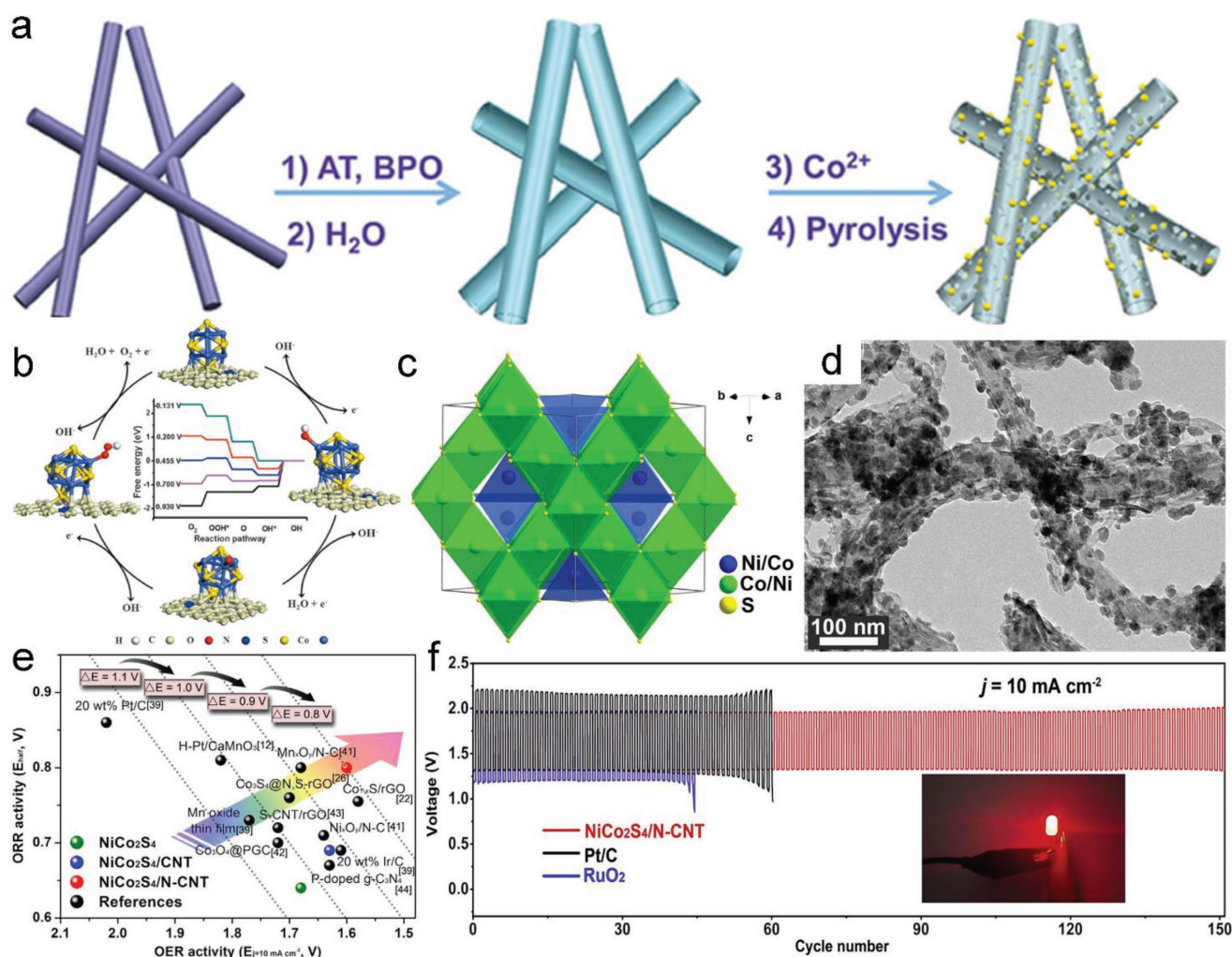


Figure 10. a) Schematic synthesis of Co₉S₈/NSPC. b) Free energy diagram of the Co₉S₈/NSPC at different applied potentials and the corresponding reaction mechanism of OER and ORR. Reproduced with permission.^[98] Copyright 2016, Springer Nature. c) Crystal structure of spinel NiCo₂S₄. d) SEM image of NiCo₂S₄/N-CNT. e) Comparison of OER and ORR bifunctional activities of samples in this work with representative electrocatalysts in references. The dotted lines show the ΔE at constant values. f) Discharge/recharge profiles of rechargeable Zn–air cells based on NiCo₂S₄/N-CNT, Pt/C, and RuO₂ cathode with duration of 400 s per cycle at 10 mA cm⁻². Reproduced with permission.^[105] Copyright 2017, Elsevier.

elements in bimetallic sulfides makes it as promising catalysts with superior catalytic activity in many chemical reactions, in which, the thiospinels AB_2S_4 is a typical family of bimetallic sulfides (Figure 10c).^[101–105] Recent researches demonstrated that Ni-doped Co–S to form thiospinel compound could display enhanced ORR/OER performance in comparison with binary Co–S composition.^[101] Throughout this field, Han et al.^[105] take a typical work, that was, an inorganic nanocarbon-coupled hybrid, homogeneous $NiCo_2S_4$ nanocrystals anchored on nitrogen-doped carbon nanotubes ($NiCo_2S_4/N-CNT$) (Figure 10d) was prepared as an extremely efficient bifunctional catalyst, the highest activity was obtained by tailoring the crystal size of $NiCo_2S_4$ in the hybrid through tuning the construction of metal–ammonia complexes. It enabled high performance of rechargeable zinc–air battery including significantly reduced charge–discharge polarization (≈ 0.63 V), enlarged energy efficiency ($\approx 67.2\%$), and prolonged cycle ability up to 150 cycles at 10 mA cm^{-2} (Figure 10e,f).

3.5. Other Catalysts

Transition-metal nitrides (TMNs) are attracting attention and have also been investigated as promising catalysts for oxygen electrode reactions due to their unique electronic properties, especially the inherent metallic character.^[106] The metallic properties are highly desirable for electrocatalytic applications, allowing very fast charge transfer between catalysts and the electrode support. Ni_3N ,^[107] Co_4N ,^[108] Ni_3FeN ,^[109,110] etc., have been proved a better electrocatalytic activity for OER than those of the corresponding oxides in alkaline medium. Chen and co-workers^[111] discovered the excellent ORR catalytic activity of vanadium nitride (VN) in alkaline environment. MoN also have an improving ORR activity due to its favorable geometry of Mo sites which can facilitate oxygen adsorption.^[112] Considering the separate OER and ORR performance of TMNs, by combining them with the opposite catalysts, some efficient bifunctional catalysts are developed. For example, Cui et al.^[113] reported an advanced bifunctional oxygen electrocatalyst consisting of porous metallic nickel–iron nitride (Ni_3FeN) supporting ordered Fe_3Pt intermetallic nanoalloy (Figure 11a–c). In this hybrid catalyst, the bimetallic nitride Ni_3FeN mainly contributed to the high activity for the OER, while the ordered Fe_3Pt nanoalloy contributed to the excellent activity for the ORR. Wang et al.^[114] replaced the precious Fe_3Pt with Co, N-codoped carbon nanoframes (Co, N-CNF) developing a 3D carbon nanoframe scaffold-immobilized Ni_3FeN nanoparticle electrocatalyst, wherein, the Ni_3FeN/Co , N-CNF hybrid afforded remarkable OER activity (overpotential of 0.27 V, superior to IrO_2) and excellent ORR performance (half-wave potential of 0.81 V vs reversible hydrogen electrode (RHE), superior to Pt/C). Fan et al.^[115] demonstrated a hybrid catalyst, of which 2D metallic Ni–Fe nitride were strongly coupled with nitrogen-doped graphene. Electronic structure of the Ni–Fe nitride was changed by hybridizing with the nitrogen-doped graphene, resulting in a unique heterostructure, leading to very high OER activity with the lowest onset overpotential (150 mV), and competitive ORR activity than commercial Pt/C (Figure 11d,e).

Except the TMNs, by combining the highly OER active catalysts with the highly ORR active ones, a series of high efficient ORR/OER bifunctional catalysts have been reported for rechargeable Zn–air batteries.^[116–120] For example, Cui et al.^[116] recently reported a durable and efficient carbide-based bifunctional catalyst consisting of iron–molybdenum carbide (Fe_3Mo_3C) and IrMn nanoalloys. This carbide was chemically stable in alkaline media and over the potential range of an air cathode, Fe_3Mo_3C was very active for ORR in alkaline media, IrMn delivered perfect OER activity, thus enabling a high energy efficiency and long-term cycling stability over 200 h in rechargeable Zn–air batteries. By combining the highly OER active $NiFe-LDH$ and $Fe-N-C$ with efficient ORR activity, Dresp et al.^[119] designed one of the today's most efficient bifunctional ORR/OER electrocatalysts, therewith, the key was a interaction of distinct neighboring active sites in the two-phase structure between these two components (Figure 11f–j). Otherwise, recently, carbon nitrides (C_3N_4) with ultrahigh N content, stable and tailorable structure and the compound have been developed as highly active bifunctional electrocatalysts for ORR and OER.^[96,121–123] About this aspect, Ma et al.^[122] fabricated a freestanding air electrode through directly growing phosphorus-doped $g-C_3N_4$ nanoflowers on carbon-fiber paper, resulting in a lot of advantages, including high specific surface area, N, P dual action, and faster mass/charge transfer, thus guaranteeing sufficient activity and stability for catalyzing reversible oxygen reactions in air electrodes for Zn–air batteries.

4. Integrated Air Electrodes and Flexible Zn–Air Batteries

In traditional steps for the fabrication of bifunctional air cathodes, catalysts are generally loaded onto a GDL framework, incorporation with the ancillary additives such as electric conduction agents (e.g., Ketjen black, acetylene black, and Super) and organic binding agents (e.g., polytetrafluoroethylene, Nafion, and Tokuyama AS4 alkaline ionomers) to hold all components together in the form of a slurry mixture through a variety of methods, such as drop-casting, screen-printing, and spray-coating, forming an interconnected conductive network.^[124] However, these additives not only make the manufacturing process complicated and a weight increase in the final electrode but also affect the battery performance negatively.^[33] First, the addition of insulating polymer binders would unavoidably increase the contact resistance between the catalytic layer and conductive substrate at their interface, thereby hindering electronic conduction, moreover, the degradation of polymeric binders in a strong caustic and oxidizing environment could lead to the peeling off of catalytic layers from the electrode surface. Second, the carbon corrosion under highly oxidative electrochemical potentials during charging complicate aggregation/sintering or even more serious leaching of catalysts. These issues sometimes severely reduce the overall battery performance. In order to circumvent these issues, an integrated binder-free air electrode will be a great solution, especially when synthesized by a combination of good conductors and high active catalysts. In addition to that, such

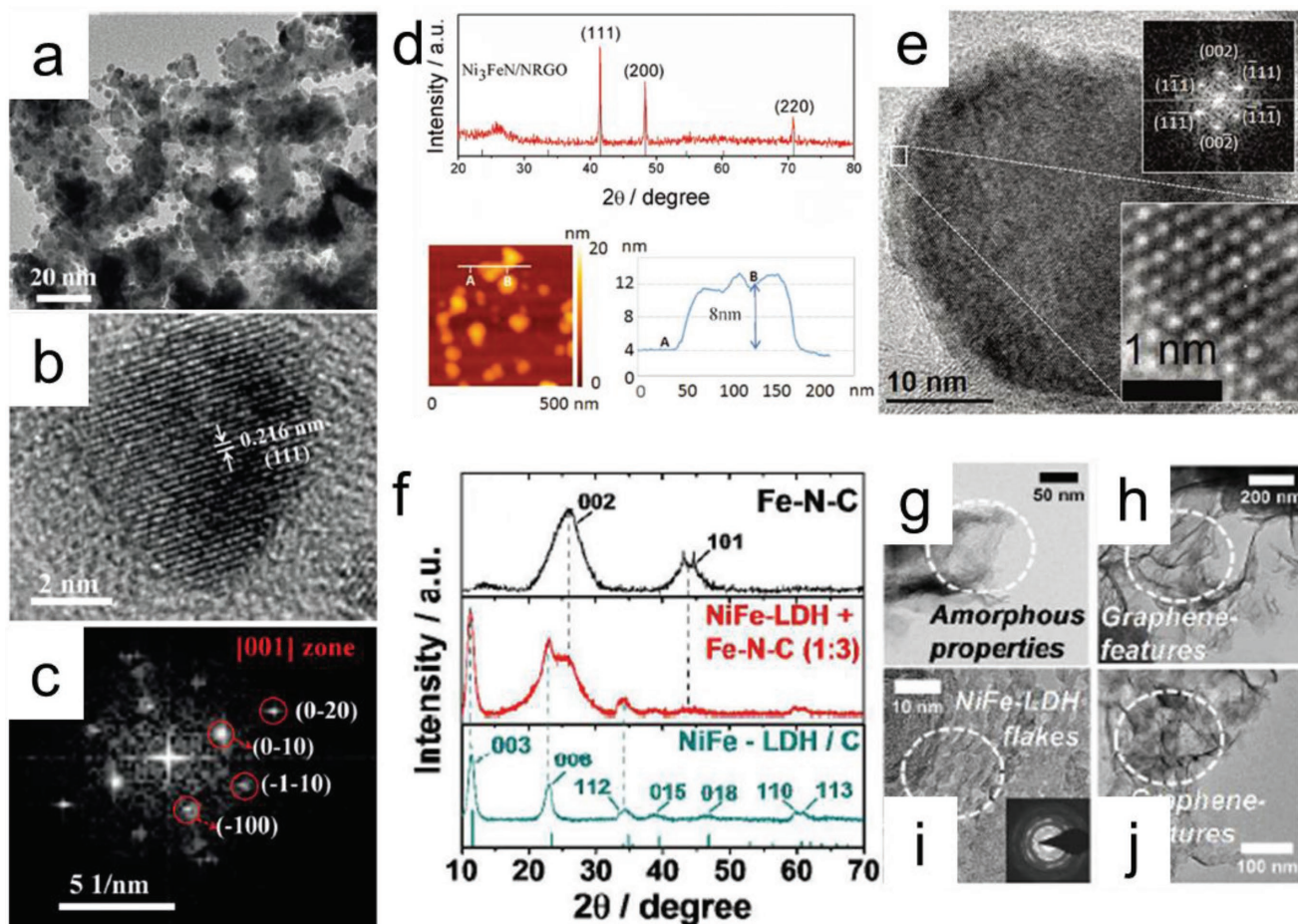


Figure 11. a) Overview TEM image of ordered $\text{Fe}_3\text{Pt}/\text{Ni}_3\text{FeN}$. b) HRTEM image of an ordered Fe_3Pt particle and c) its corresponding fast fourier transform (FFT) image of the atomic arrangement highlighting the lattice reflections. Reproduced with permission.^[113] Copyright 2017, Wiley. d) XRD pattern and atomic force microscopy (AFM) image and cross-sectional profile and e) bright-field (BF)-HRTEM image of the $\text{Ni}_3\text{FeN}/\text{N}$ -doped reduced graphene oxide (NRGO) hybrid catalyst. Reproduced with permission.^[115] Copyright 2017, Wiley. f) XRD patterns of $\text{NiFe-LDH}/\text{C}$. TEM images of g,h) Fe-N-C and i,j) $\text{NiFe-LDH}/\text{C}$. Reproduced with permission.^[119] Copyright 2016, Royal Society of Chemistry.

integrative bifunctional air electrodes are directly fabricated on current collectors (conductive substrates) as a whole, there is no complex preparation processes compared to traditional methods, appearing to be convenient, cheap, and suitable for large-scale fabrication. In addition to that, a number of recent studies have focused on flexible Zn-air batteries with a variety of structures to meet the rapidly growing new wave of smart-wearable technologies and wireless communications due to the high energy density and environment friendliness.^[8,125–131] So, the flexible Zn-air batteries will no doubt bring new demands to the stable operation under bending conditions. In order to realize that, integrated freestanding air electrodes with flexible substrates is essential. Table 1 summarizes some recently reported integrated bifunctional air electrodes. The open circle potential, voltage gap between the discharge and charge, and the durability are compared to evaluate the differences of their overall air-electrode performance. The recently reported integrative bifunctional air electrodes for electrically rechargeable zinc-air batteries are mainly fabricated on conductive carbon and metal substrates, which are summarized and reviewed separately.

4.1. Carbon Substrates

Carbon cloth (CC),^[132,133] carbon paper,^[122] are the most commonly used substrates, which are commercially available, and have high mechanical strength and conductivity. Recently, Chen et al.^[132] successfully developed a binder-free and facile method for in situ growth of ultrathin mesoporous Co_3O_4 layers with maximum contact area on the surface of carbon fibers in the carbon cloth as high-performance air electrode for the flexible rechargeable Zn-air batteries (Figure 12a–c). The ultrathin $\text{Co}_3\text{O}_4/\text{CC}$ electrode showed superior catalytic performance for ORR and OER and the corresponding activity was more than 10 times higher than that of the commercial $\text{Co}_3\text{O}_4/\text{CC}$ electrode. The flexible Zn-air battery using ultrathin $\text{Co}_3\text{O}_4/\text{CC}$ electrode exhibited excellent rechargeable performance (Figure 12d–f). By one step heat treatment of synthesized pearl-like ZIF-67/polypyrrole nanofiber network, our group in situ coupled strung Co_4N and intertwined N-C fibers rooted on carbon cloth to build a freestanding bifunctional air electrode of Co_4N , carbon fibers network, and carbon cloth ($\text{Co}_4\text{N}/\text{CNW}/\text{CC}$) (Figure 12g–i).^[133] Originating from the high OER activity of Co_4N and ORR activity

Table 1. Zn–air batteries performance of some recent reports of integrated air electrodes.

| Air electrode | Feature (cell structure) | Electrolyte | Open circuit potential | Voltage gap | Durability | Ref. |
|--|--------------------------|---|------------------------|-------------|--|-------|
| ultrathin $\text{Co}_3\text{O}_4/\text{CC}$ | Flexible (flexible) | polyvinyl alcohol–KOH (PVA–KOH) hydrogel | 1.33 V | 0.92 V | 30 cycles for 10 h@2 mA cm ⁻² | [132] |
| $\text{Co}_4\text{N}/\text{CNW}/\text{CC}$ | Flexible (flexible) | PVA–KOH hydrogel | 1.35 V | NA | 36 cycles for 12 h@1 mA cm ⁻² | [133] |
| NCNF-1000 | Flexible (flexible) | PVA–KOH hydrogel | 1.26 V | 0.78 V | 48 cycles for 6 h@2 mA cm ⁻² | [135] |
| $\text{Co}_3\text{O}_4/\text{N-CNT}$ aerogel | Flexible (flexible) | PVA–KOH hydrogel | NA | 1.0 V | 20 cycles for 20 h@2 mA cm ⁻² | [136] |
| CNT sheets | Flexible (flexible) | PVA–polyethylene oxide (PEO)–KOH hydrogel | 1.29 V | NA | 30 cycles for 30 h@1 A g ⁻¹ | [137] |
| $\text{Co}_3\text{O}_4\text{-N-CNT}/\text{SS}$ | Flexible (flexible) | Cellulose film/6 M KOH | NA | 0.72 V | 1800 cycles for 600 h@25 mA cm ⁻² | [143] |
| C–CoPAN900 | Flexible (rigid) | 6 M KOH | NA | 0.7 V | 157 cycles for 157 h@2 mA cm ⁻² | [138] |
| N8-VA-CNTs/graphene foam (GF) | Flexible (rigid) | 6 M KOH | NA | 0.87 V | 240 cycles for 240 h@10 mA cm ⁻² | [134] |
| Co_3O_4 NW | Flexible (rigid) | 6 M KOH | NA | 1.1 V | 100 cycles for 600 h@50 mA ⁻² | [142] |

of Co–N–C as well as a stable 3D-interconnected conductive network, the $\text{Co}_4\text{N}/\text{CNW}/\text{CC}$ electrode presented high efficiency and stability in the assembled rechargeable Zn–air batteries with a low discharge–charge overpotential (1.09 V at 50 mA cm⁻²) and 408 pulse cycles (Figure 12j). Except the commercial carbon substrates, some homemade integrated carbon substrates have also been developed.^[134–138] For instance, Li and co-workers^[136] utilized a lightweight, conductive, and cross-linked aerogel film of CNTs functioning as a 3D catalyst-supporting scaffold for bifunctional cobalt (II/III) oxides and as a current collector (Figure 13a,b). By thermal carbonization of electrospun polymer fibers containing metal ion, Co_3O_4 nanoparticle–decorated carbon nanofibers were prepared and worked as an efficient bifunctional air electrodes to accelerate the charging–discharging

process (Figure 13c–e).^[138] Liu et al.^[135] newly developed a free-standing metal-free nanoporous carbon nanofiber films (NCNF) electrode with large specific surface area, bifunctional activity, and flexibility used in a Zn–air battery (Figure 13f), wherein, the battery could get high reversibility (an initial round-trip efficiency of 62%) and stability as long as 500 cycles with a voltage gap increase of only 130 mV (Figure 13g).

4.2. Metal Substrates

Integrated air electrodes built on carbon-based substrates have achieved great development; lightweight and easy fabrication are the advantages of carbon substrates, however, carbon

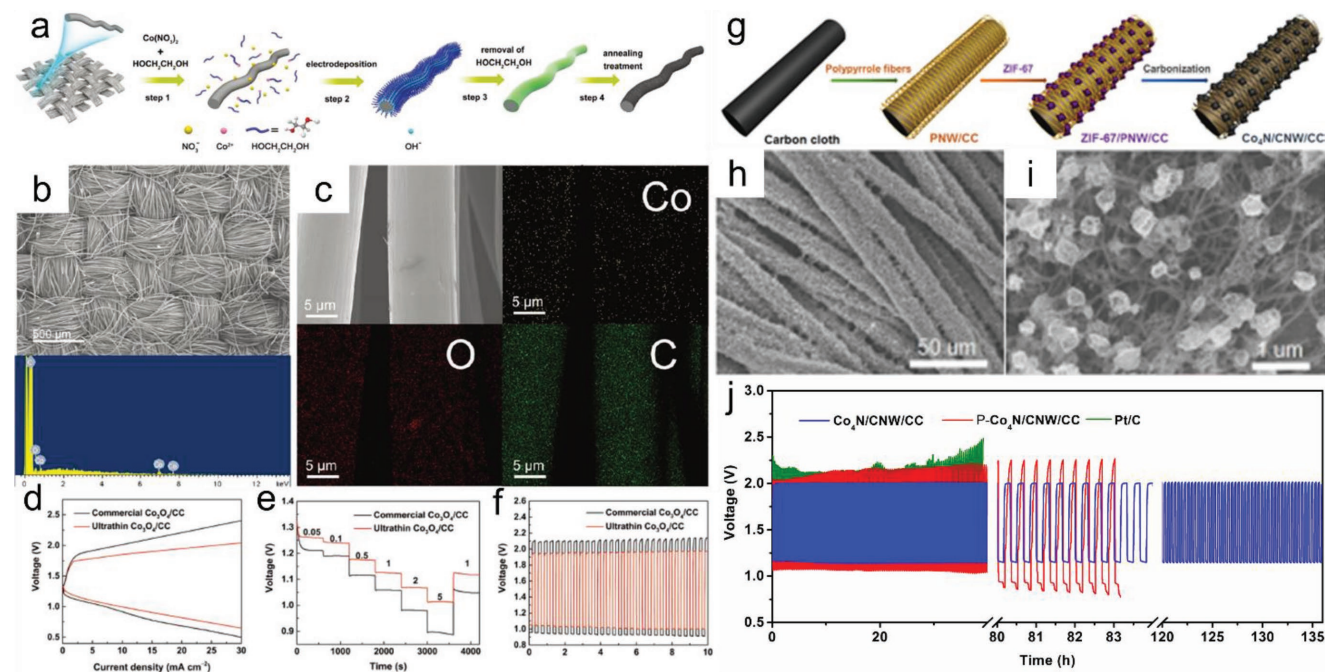


Figure 12. a) Schematic diagram of the preparation procedure, b) the SEM image, and c) energy dispersive spectroscopy (EDS) elemental analysis of $\text{Co}_3\text{O}_4/\text{CC}$. d–f) The performance of the flexible Zn–air battery using ultrathin $\text{Co}_3\text{O}_4/\text{CC}$ electrode. Reproduced with permission.^[132] Copyright 2017, Wiley. g) Scheme of the synthesis of $\text{Co}_4\text{N}/\text{CNW}/\text{CC}$. h, i) SEM images of $\text{Co}_4\text{N}/\text{CNW}/\text{CC}$. j) Cycling curves at 10 mA cm⁻² of the rechargeable Zn–air batteries with the $\text{Co}_4\text{N}/\text{CNW}/\text{CC}$ electrode. Reproduced with permission.^[133] Copyright 2016, American Chemical Society.

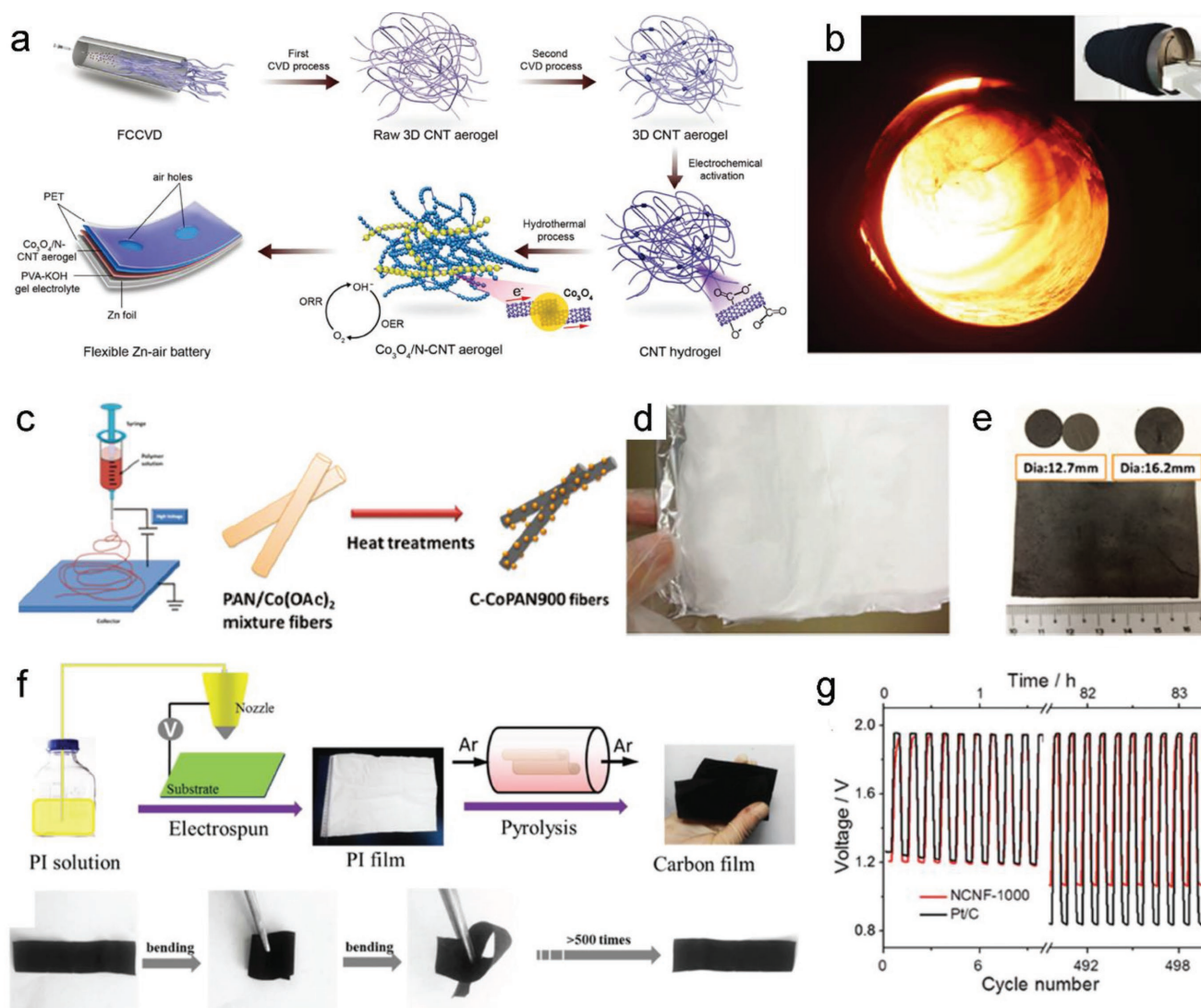


Figure 13. a) Schematic showing the preparation of $\text{Co}_3\text{O}_4/\text{N-CNT}$ composite aerogel films utilized for freestanding electrode of zinc–air batteries. b) Photograph showing the raw CNT aerogel fabricated by floating chemical vapor deposition (FCCVD) method (the inset figure showing the as-collected raw CNT aerogel on a mandrel).^[136] c) Schematic illustration of C–CoPAN hybrid catalyst nanofibers. d) Photographs of the electrospun polyacrylonitrile (PAN) nanofibers and e) freestanding carbonized electrospun nanofibers. Reproduced with permission.^[138] Copyright 2014, Royal Society of Chemistry. f) Scheme and photographs of flexible NCNF. g) Cycling curves of rechargeable Zn–air batteries with the NCNF-1000 and Pt/C air electrodes.^[135]

corrosion under high oxidation potential during charging process is more or less unavoidable, despite their high graphitization degree, thus leading to attenuation performance of the assembled batteries.^[18,21,139] Accordingly, it is crucial to prevent the destruction of air electrodes induced by corrosion of carbon substrates to improve the stability of air electrodes for long-term operation. Titanium mesh, stainless-steel (SS) mesh, and nickel foam as metal-based substrates with high-electrical conductivity and electro-oxidation stability are very suitable candidates, directly growing nanostructured electrocatalysts on them is perhaps an effective approach.^[139–143] For instance, Li and Manthiram^[141] decoupled IrO_2 thin films grown onto a Ti mesh (IrO_2/Ti) for OER and a commercial Pt/C catalyst on a GDL for ORR. The SS mesh–based integration of electrodes were developed widely, for instance, Lee et al.^[142] proposed an

advanced highly active ORR/OER bifunctional air electrode through directly coupling hierarchical mesoporous Co_3O_4 NW arrays on an underlying SS mesh without using any ancillary material (Figure 14a,b). In comparison with conventional GDL electrodes, the battery of Co_3O_4 NW/SS exhibited a much lower gap of charge–discharge voltages accompanied with 1500 pulse cycles at high currents without significant performance degradation. In this electrode, nonconductive ancillary polymer binders and additional active carbons are wiped off, circumventing the decomposition of binders and carbon corrosion, and improving the electrical property and electrochemical stability. For further exploitation of SS mesh–based air electrodes with high bifunctional catalytic performance, recently, Fu et al.^[143] developed a freestanding bifunctional air electrode by morphological emulation of a human-hair array, which was directly constructed on a

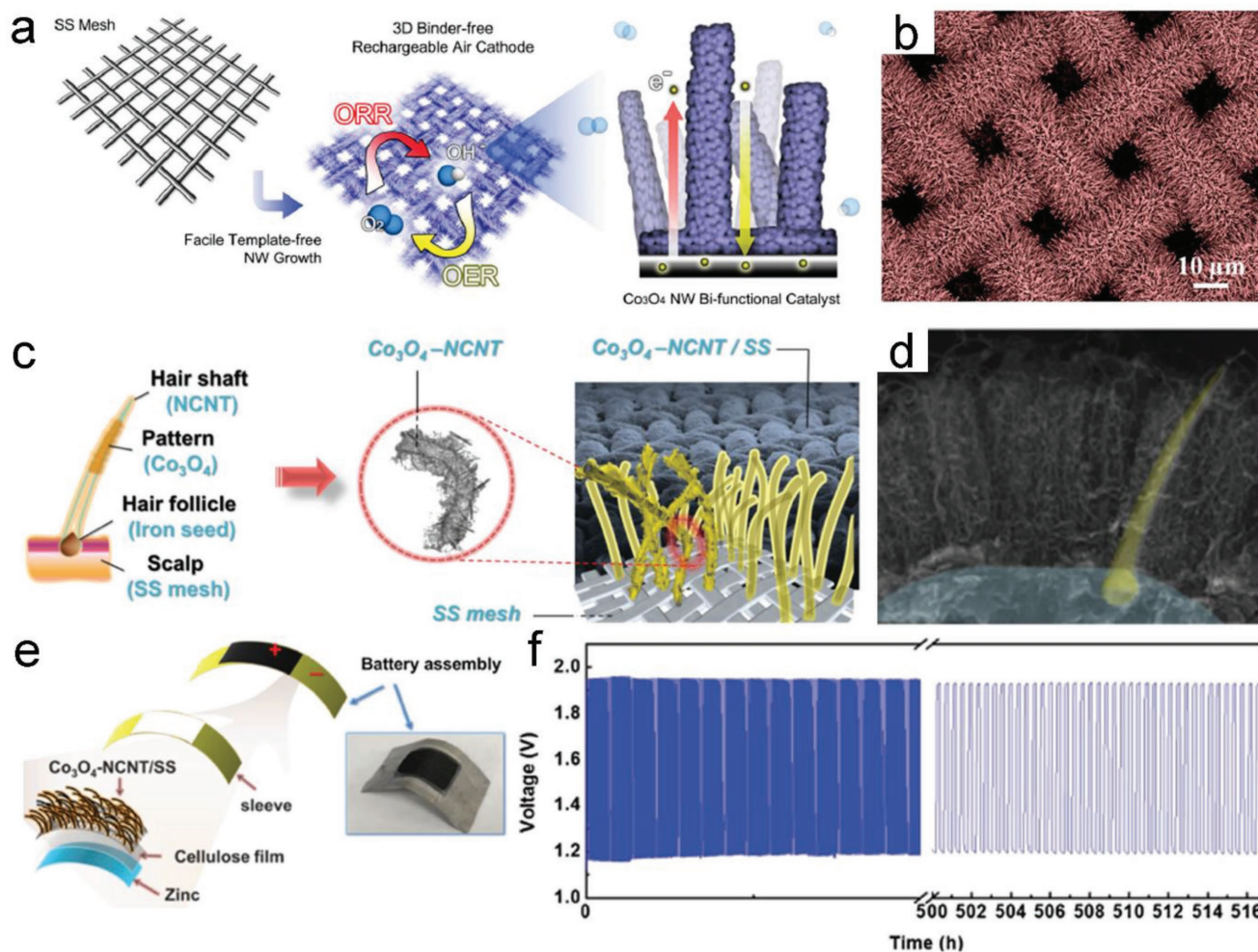


Figure 14. a) Schematic illustration of Co₃O₄ NW. b) The corresponding SEM image. Reproduced with permission.^[142] Copyright 2014, Wiley-VCH. c) Schematic illustration of Co₃O₄-N-CNT/SS air electrode. d) The corresponding SEM image. e) Scheme of the flexible solid-state Zn-air battery. f) Charge-discharge cycling curves. Reproduced with permission.^[143] Copyright 2016, Wiley-VCH.

SS mesh with a hair-like bifunctional catalysts array containing a nanoassembly of mesoporous Co₃O₄ nanopetals in N-CNTs vertically grown (Figure 14c,d). An intimate interfacial contact between Co₃O₄ and N-CNT formed in this hair-like structure of the Co₃O₄-N-CNT nanoassembly, which could favor a low electron transfer impedance and a high flux of mass transfer during the catalytic process. Besides, the decoration of Co₃O₄ helped to improve the wettability of the air electrode, hence, facilitating the diffusion of oxygen inside the electrode. The assembled solid-state Zn-air battery based on the Co₃O₄-N-CNT/SS air electrode (Figure 14e) reached a high energy density and perfect cycling stability as long as 600 h under a high current density of 25 mA cm⁻² (Figure 14f).

5. Conclusion and Outlook

In conclusion, in the energy storage field, the Zn-air battery holds the potential to be the energy supplier of the next generalization, benefiting from its high energy density. Rational-designed air electrodes with bifunctional ORR/OER catalytic

activity are critical for rechargeable Zn-air batteries, because a lot of key physical and chemical processes including redox electrochemical reactions of oxygen, heat and mass transfer, flow distribution, chemical kinetics, oxygen storage and release, catalyst deactivation, etc., take place in the air electrodes. The oxygen-related reactions during the charging and discharging cycles involving multistep electron transfer which are very complicated involving many continuous complex electrochemical reactions and kinetically slow, in order to accelerate that for practically use of rechargeable Zn-air batteries, bifunctional catalysts are very necessary. The mass transfer, flow distribution, and catalyst deactivation are greatly influenced by the structure of air electrodes, in which, an optimal gas-electrolyte-catalyst three-phase interface must be created in the GDL with the help of hydrophilic and hydrophobic microchannels. Recent-developed typical nonprecious metal-based ORR/OER bifunctional catalysts are also summarized briefly and systematically in this review (Table 2), including heteroatom-doped nanostructured carbonaceous materials, metal nanoparticles encapsulated in carbon layer, metal oxides, metal chalcogenides, and their nanocarbon hybrid materials, as well

Table 2. Zn–air batteries performance of some recent reports of non-noble-metal catalysts.

| Air catalysts | Electrolytes | Open circuit potential | Power density | Specific capacity | Voltage gap | Durability | Ref. |
|---|--------------|------------------------|---------------------------|--|-------------|--|-------|
| NPMC-1000 | 6 M KOH | 1.48 V | 55 mW cm ⁻² | 735 mAh g ⁻¹ @5 mA cm ⁻² | NA | 600 cycles for 100 h@2 mA cm ⁻² | [29] |
| N-doped graphene nanoribbon networks (N-GRW) | 6 M KOH | 1.46 V | 65 mW cm ⁻² | 873 mAh g ⁻¹ @5 mA cm ⁻² | 0.8 V | 150 cycles for 150 h@2 mA cm ⁻² | [34] |
| Fe@N-C-700 | 6 M KOH | 1.4 V | 157 mW cm ⁻² | NA | 0.7 V | 100 cycles for 17 h@10 mA cm ⁻² | [57] |
| Three-dimensional actiniae-like carbon nanotube assembly (3D-CNTA) | 6 M KOH | 1.41 V | 157.3 mW cm ⁻² | NA | 0.68 V | 240 cycles for 40 h@10 mA cm ⁻² | [65] |
| NiFe@NC _x | 6 M KOH | 1.36 V | NA | 732.3 mAh g ⁻¹ @10 mA cm ⁻² | 0.39 V | 205 cycles for 34 h@10 mA cm ⁻² | [71] |
| 3D ordered mesoporous (3DOM) Co ₃ O ₄ | 6 M KOH | 1.36 V | NA | NA | 0.76 V | 200 cycles for 400 h@10 mA cm ⁻² | [74] |
| La-(Co _{0.71} Ni _{0.25}) _{0.96} O _{3-δ} | 6 M KOH | 1.45 V | NA | 705 mAh g ⁻¹ @5 A g ⁻¹ | 0.53 V | 20 cycles for 3.2 h@5 A g ⁻¹ | [79] |
| CoO/N-CNT and FeNi LDH/CNT | 6 M KOH | 1.4 V | 265 mW cm ⁻² | 575 mAh g ⁻¹ @10 mA cm ⁻² | NA | 100 cycles for 200 h@20 mA cm ⁻² | [30] |
| Fe _{0.5} Co _{0.5} O _x /N-doped reduced graphene oxide (NrGO) | 6 M KOH | 1.44 V | 86 mW cm ⁻² | 756 mAh g ⁻¹ @10 mA cm ⁻² | 0.79 V | 60 cycles for 120 h@10 mA cm ⁻² | [85] |
| ZnCo ₂ O ₄ /N-CNT | 6 M KOH | 1.47 V | 82.3 mW cm ⁻² | 428.47 mAh g ⁻¹ @10 mA cm ⁻² | 0.84 V | 17 cycles for 5.7 h@10 mA cm ⁻² | [88] |
| CuCo ₂ O ₄ /N-CNTs | 6 M KOH | 1.36 V | 83.83 mW cm ⁻² | 871.4 mAh g ⁻¹ @100 mA cm ⁻² | 0.36 V | 240 cycles for 40 h@20 mA cm ⁻² | [89] |
| Co ₃ FeS _{1.5} (OH) ₆ | 6 M KOH | NA | 113.1 mW cm ⁻² | 898 mAh g ⁻¹ @20 mA cm ⁻² | 0.84 V | 108 cycles for 36 h@2 mA cm ⁻² | [96] |
| CuS/NiS ₂ INs | 6 M KOH | 1.44 V | 172.4 mW cm ⁻² | 775 mAh g ⁻¹ @5 mA cm ⁻² | 0.57 V | 500 cycles for 83 h@25 mA cm ⁻² | [97] |
| NiCo ₂ S ₄ /N-CNT | 6 M KOH | 1.49 V | 147 mW cm ⁻² | 431 mAh g ⁻¹ @5 mA cm ⁻² | 0.63 V | 150 cycles for 16.7 h@10 mA cm ⁻² | [105] |
| Ni ₃ FeN/Co, NCNF | 6 M KOH | 1.43 V | 200 mW cm ⁻² | NA | 0.79 V | 540 cycles for 540 h@6 mA cm ⁻² | [114] |
| NiO/CoN porous NiO/CoN interface nanowire arrays (PINWs) | 6 M KOH | 1.46 V | 79.6 mW cm ⁻² | 690 mAh g ⁻¹ @5 mA cm ⁻² | 0.84 V | 50 cycles for 8.3 h@1 mA cm ⁻² | [117] |
| CoP@mNSP-C | 6 M KOH | NA | 124 mW cm ⁻² | NA | 0.61 V | 100 cycles for 450 h@1 mA cm ⁻² | [120] |
| P, S-carbon nitride sponges (CNS) | 6 M KOH | 1.51 V | 198 mW cm ⁻² | 830 mAh g ⁻¹ @5 mA cm ⁻² | 0.8 V | 500 cycles for 100 h@25 mA cm ⁻² | [121] |

as some successful combination of the highly OER and ORR active catalysts.

Despite these diverse efficient bifunctional candidates, throughout these catalysts and air electrodes, carbon materials are almost indispensable, whether as conductive additives and substrates, active catalysts, or functional materials coupled with metal-based species, realizing improved conductivity and unexpected synergistic coupling effect. In this case, carbon corrosion under high oxidation potential during charging process is unavoidable. This results in the loss of catalysts and reduced performance, leading to low stability. In order to minimize it, highly graphitized carbon materials and metal mesh are employed, which can restrain the corrosion effect in the cycling for highly efficient air electrodes. It is also a key strategy to develop high OER active metal-based catalysts to reduce charge potential. In the design of all these kind of catalysts, morphology control is an important factor, which can greatly influence a catalyst's properties, such as the specific surface area, in turn, to tune the catalytic behavior. Maximizing the performance of air cathodes by combining 1D, 2D, and 3D dimensions for the rational design of the catalyst structure to construct

hierarchical-structured air catalysts is of significant importance. Using MOFs as efficient precursors to synthesize carbon- or metal-based catalysts with multidimensional hierarchical structures has been developed as an important strategy.^[144–146] Besides, recent researches further develop various integrated binder-free air cathodes to solve another problem of the degradation of polymeric binders, so that, directly growing high active catalysts on highly corrosion-resistant carbon materials or metallic meshes/foams is suggested as novel efficient strategies. Not only that, such approaches are very suitable for large-scale production, benefitting from free of the traditional complex preparation processes. An integrated air cathode with 3D hierarchical structure can provide smaller electrical resistance and shorter ion diffusion pathways, thus facilitating fast ion and electron transportation. However, some new issues such as the utilizable of active materials and electrolyte penetration for these air electrodes following needs to be considered, especially when using metal foam or mesh as the substrate.

As a solution, it is necessary to establish hydrophobic microchannels to prevent electrolyte leaking out, the integrated electrode itself also should have suitable hydrophilic microchannels,

allowing the infiltration of the liquid electrolyte to create gas–electrolyte–catalyst three-phase interface for the ORR and OER process. Using gel polymer electrolytes, novel battery configurations with a solid-state form can avoid electrolyte penetration, in spite of high ionic conductivities, the possible evaporation liquid in gel and limited reaction boundaries will restrict their performance and long-term application that should be resolved. Across the board, benefitting from advantages of low cost, high energy density, and safety, rechargeable zinc–air batteries are competitive and meet the rapidly increasing demand for clean energy, the relative rational-designed bifunctional air electrodes are becoming more and more critical, and expected to command much more attention.

Acknowledgements

This work was financially supported by the Ministry of Science and Technology of the People's Republic of China (Grant Nos. 2016YFB0100103 and 2017YFA0206704), the National Program on Key Basic Research Project of China (2014CB932300), the Strategic Priority Research Program of the Chinese Academy of Sciences (Grant No. XDA09010404), the Technology and Industry for National Defense of the People's Republic of China (Grant No. JCKY2016130B010), and the National Natural Science Foundation of China (51771177, 21422108, and 51472232).

Conflict of Interest

The authors declare no conflict of interest.

Keywords

air electrodes, bifunctional, electrocatalysts, rechargeable Zn–air batteries

Received: November 4, 2017
Revised: February 17, 2018
Published online: July 12, 2018

- [1] J. Zhang, Z. Xia, L. Dai, *Sci. Adv.* **2015**, *1*, e1500564.
- [2] P. Chen, T. Zhou, L. Xing, K. Xu, Y. Tong, H. Xie, L. Zhang, W. Yan, W. Chu, C. Wu, Y. Xie, *Angew. Chem., Int. Ed.* **2017**, *56*, 610.
- [3] C. Meng, T. Ling, T. Y. Ma, H. Wang, Z. Hu, Y. Zhou, J. Mao, X. W. Du, M. Jaroniec, S. Z. Qiao, *Adv. Mater.* **2017**, *29*, 1604607.
- [4] J.-I. Jung, M. Risch, S. Park, M. G. Kim, G. Nam, H.-Y. Jeong, Y. Shao-Horn, J. Cho, *Energy Environ. Sci.* **2016**, *9*, 176.
- [5] X. Wang, F. Wang, L. Wang, M. Li, Y. Wang, B. Chen, Y. Zhu, L. Fu, L. Zha, L. Zhang, Y. Wu, W. Huang, *Adv. Mater.* **2016**, *28*, 4904.
- [6] S. Qu, Z. Song, J. Liu, Y. Li, Y. Kou, C. Ma, X. Han, Y. Deng, N. Zhao, W. Hu, C. Zhong, *Nano Energy* **2017**, *39*, 101.
- [7] J. Park, M. Risch, G. Nam, M. Park, T. J. Shin, S. Park, M. G. Kim, Y. Shao-Horn, J. Cho, *Energy Environ. Sci.* **2017**, *10*, 129.
- [8] J. Park, M. Park, G. Nam, J.-S. Lee, J. Cho, *Adv. Mater.* **2015**, *27*, 1396.
- [9] Y. Zhao, Q. Lai, Y. Wang, J. Zhu, Y. Liang, *ACS Appl. Mater. Interfaces* **2017**, *9*, 16178.
- [10] Z. K. Yang, L. Lin, A. W. Xu, *Small* **2016**, *12*, 5710.
- [11] M. Xu, D. G. Ivey, Z. Xie, W. Qu, *J. Power Sources* **2015**, *283*, 358.
- [12] J. Zhang, L. Qu, G. Shi, J. Liu, J. Chen, L. Dai, *Angew. Chem., Int. Ed.* **2016**, *55*, 2230.
- [13] J. Park, M. Park, G. Nam, M. G. Kim, J. Cho, *Nano Lett.* **2017**, *17*, 3974.
- [14] H. W. Liang, X. Zhuang, S. Bruller, X. Feng, K. Mullen, *Nat. Commun.* **2014**, *5*, 4973.
- [15] L. Dai, Y. Xue, L. Qu, H. J. Choi, J. B. Baek, *Chem. Rev.* **2015**, *115*, 4823.
- [16] K. N. Ferreira, T. M. Iverson, K. Maghlaoui, J. Barber, S. Iwata, *Science* **2004**, *303*, 1831.
- [17] J. Rossmesl, Z.-W. Qu, H. Zhu, G.-J. Kroes, J. K. Nørskov, *J. Electrochem. Soc.* **2007**, *607*, 83.
- [18] X. Cai, L. Lai, J. Lin, Z. Shen, *Mater. Horiz.* **2017**, *4*, 945.
- [19] M. S. Burke, L. J. Enman, A. S. Batchellor, S. Zou, S. W. Boettcher, *Chem. Mater.* **2015**, *27*, 7549.
- [20] D. U. Lee, P. Xu, Z. P. Cano, A. G. Kashkooli, M. G. Park, Z. Chen, *J. Mater. Chem. A* **2016**, *4*, 7107.
- [21] J. Fu, Z. P. Cano, M. G. Park, A. Yu, M. Fowler, Z. Chen, *Adv. Mater.* **2017**, *29*, 1604685.
- [22] J. Ge, A. Higier, H. Liu, *J. Power Sources* **2006**, *159*, 922.
- [23] H. Su, Q. Xu, J. Chong, H. Li, C. Sita, S. Pasupathi, *J. Power Sources* **2017**, *341*, 302.
- [24] H. Sadeghifar, N. Djalili, M. Bahrami, *J. Power Sources* **2014**, *248*, 632.
- [25] S. Suren, S. Kheawhom, *J. Electrochem. Soc.* **2016**, *163*, A846.
- [26] W.-M. Yan, C.-Y. Hsueh, C.-Y. Soong, F. Chen, C.-H. Cheng, S.-C. Mei, *Int. J. Hydrogen Energy* **2007**, *32*, 4452.
- [27] E. Deiss, F. Holzer, O. Haas, *Electrochim. Acta* **2002**, *47*, 3995.
- [28] S. W. Price, S. J. Thompson, X. Li, S. F. Gorman, D. Pletcher, A. E. Russell, F. C. Walsh, R. G. Wills, *J. Power Sources* **2014**, *259*, 43.
- [29] J. Zhang, Z. Zhao, Z. Xia, L. Dai, *Nat. Nanotechnol.* **2015**, *10*, 444.
- [30] Y. Li, M. Gong, Y. Liang, J. Feng, J. E. Kim, H. Wang, G. Hong, B. Zhang, H. Dai, *Nat. Commun.* **2013**, *4*, 1805.
- [31] Y. Li, H. Dai, *Chem. Soc. Rev.* **2014**, *43*, 5257.
- [32] X. Liu, M. Park, M. G. Kim, S. Gupta, G. Wu, J. Cho, *Angew. Chem., Int. Ed.* **2015**, *54*, 9654.
- [33] C. Tang, B. Wang, H.-F. Wang, Q. Zhang, *Adv. Mater.* **2017**, *29*, 1703185.
- [34] H. B. Yang, J. Miao, S.-F. Hung, J. Chen, H. B. Tao, X. Wang, L. Zhang, R. Chen, J. Gao, H. M. Chen, *Sci. Adv.* **2016**, *2*, e1501122.
- [35] H. X. Zhong, J. Wang, Q. Zhang, F. Meng, D. Bao, T. Liu, X. Y. Yang, Z. W. Chang, J. M. Yan, X. B. Zhang, *Adv. Sustainable Syst.* **2017**, *1*, 1700020.
- [36] B. Li, D. Geng, X. S. Lee, X. Ge, J. Chai, Z. Wang, J. Zhang, Z. Liu, T. S. Hor, Y. Zong, *Chem. Commun.* **2015**, *51*, 8841.
- [37] Y. Zhao, L. Yang, S. Chen, X. Wang, Y. Ma, Q. Wu, Y. Jiang, W. Qian, Z. Hu, *J. Am. Chem. Soc.* **2013**, *135*, 1201.
- [38] Y. Qian, Z. H. , X. Ge, S. Yang, Y. Peng, Z. Kang, Z. Liu, J. Y. Lee, D. Zhao, *Carbon* **2017**, *111*, 641.
- [39] N. Daems, X. Sheng, I. F. Vankelecom, P. P. Pescarmona, *J. Mater. Chem. A* **2014**, *2*, 4085.
- [40] C. Zhang, N. Mahmood, H. Yin, F. Liu, Y. Hou, *Adv. Mater.* **2013**, *25*, 4932.
- [41] S. Patra, R. Choudhary, E. Roy, R. Madhuri, P. K. Sharma, *Nano Energy* **2016**, *30*, 118.
- [42] Z. Ma, S. Dou, A. Shen, L. Tao, L. Dai, S. Wang, *Angew. Chem., Int. Ed.* **2015**, *54*, 1888.
- [43] K. Ai, Y. Liu, C. Ruan, L. Lu, G. M. Lu, *Adv. Mater.* **2013**, *25*, 998.
- [44] B. Y. Xia, Y. Yan, N. Li, H. B. Wu, X. W. Lou, X. Wang, *Nat. Energy* **2016**, *1*, 15006.
- [45] S. Chen, J. Duan, Y. Zheng, X. Chen, X. W. Du, M. Jaroniec, S.-Z. Qiao, *Energy Storage Mater.* **2015**, *1*, 17.
- [46] Y. Su, Z. Yao, F. Zhang, H. Wang, Z. Mics, E. Cánovas, M. Bonn, X. Zhuang, X. Feng, *Adv. Funct. Mater.* **2016**, *26*, 5893.
- [47] K. Qu, Y. Zheng, S. Dai, S. Z. Qiao, *Nano Energy* **2016**, *19*, 373.

- [48] Q. Tang, L. Wang, M. Wu, N. Xu, L. Jiang, J. Qiao, *J. Power Sources* **2017**, 365, 348.
- [49] J. Zhang, H. Zhou, J. Zhu, P. Hu, C. Hang, J. Yang, T. Peng, S. Mu, Y. Huang, *ACS Appl. Mater. Interfaces* **2017**, 9, 24545.
- [50] Z. Zhao, M. Li, L. Zhang, L. Dai, Z. Xia, *Adv. Mater.* **2015**, 27, 6834.
- [51] C.-Y. Su, H. Cheng, W. Li, Z.-Q. Liu, N. Li, Z. Hou, F.-Q. Bai, H.-X. Zhang, T.-Y. Ma, *Adv. Energy Mater.* **2017**, 7, 1602420.
- [52] J. Song, C. Zhu, S. Fu, Y. Song, D. Du, Y. Lin, *J. Mater. Chem. A* **2016**, 4, 4864.
- [53] M. Zeng, Y. Liu, F. Zhao, K. Nie, N. Han, X. Wang, W. Huang, X. Song, J. Zhong, Y. Li, *Adv. Funct. Mater.* **2016**, 26, 4397.
- [54] G. Nam, J. Park, M. Choi, P. Oh, S. Park, M. G. Kim, N. Park, J. Cho, J.-S. Lee, *ACS Nano* **2015**, 9, 6493.
- [55] S. Gadipelli, T. Zhao, S. A. Shevlin, Z. Guo, *Energy Environ. Sci.* **2016**, 9, 1661.
- [56] Y. Liu, F. Chen, W. Ye, M. Zeng, N. Han, F. Zhao, X. Wang, Y. Li, *Adv. Funct. Mater.* **2017**, 27, 1606034.
- [57] J. Wang, H. Wu, D. Gao, S. Miao, G. Wang, X. Bao, *Nano Energy* **2015**, 13, 387.
- [58] S. Liu, Z. Wang, S. Zhou, F. Yu, M. Yu, C. Y. Chiang, W. Zhou, J. Zhao, J. Qiu, *Adv. Mater.* **2017**, 29, 1700874.
- [59] Z.-L. Wang, D. Xu, H.-X. Zhong, J. Wang, F.-L. Meng, X.-B. Zhang, *Sci. Adv.* **2015**, 1, e1400035.
- [60] M. Antonietti, N. Fechner, T.-P. Feller, *Chem. Mater.* **2014**, 26, 196.
- [61] G. Fu, Y. Chen, Z. Cui, Y. Li, W. Zhou, S. Xin, Y. Tang, J. B. Goodenough, *Nano Lett.* **2016**, 16, 6516.
- [62] H. Furukawa, K. E. Cordova, M. O'Keeffe, O. M. Yaghi, *Science* **2013**, 341, 1230444.
- [63] J. Tang, R. R. Salunkhe, J. Liu, N. L. Torad, M. Imura, S. Furukawa, Y. Yamauchi, *J. Am. Chem. Soc.* **2015**, 137, 1572.
- [64] W. Chaikittisilp, N. L. Torad, C. Li, M. Imura, N. Suzuki, S. Ishihara, K. Ariga, Y. Yamauchi, *Chem. - Eur. J.* **2014**, 20, 4217.
- [65] S. Wang, J. Qin, T. Meng, M. Cao, *Nano Energy* **2017**, 39, 626.
- [66] M. Wang, T. Qian, J. Zhou, C. Yan, *ACS Appl. Mater. Interfaces* **2017**, 9, 5213.
- [67] T. Meng, J. Qin, S. Wang, D. Zhao, B. Mao, M. Cao, *J. Mater. Chem. A* **2017**, 5, 7001.
- [68] B. Y. Guan, L. Yu, X. W. D. Lou, *Energy Environ. Sci.* **2016**, 9, 3092.
- [69] S. Zhao, H. Yin, L. Du, L. He, K. Zhao, L. Chang, G. Yin, H. Zhao, S. Liu, Z. Tang, *ACS Nano* **2014**, 8, 12660.
- [70] J.-S. Lee, G. Nam, J. Sun, S. Higashi, H.-W. Lee, S. Lee, W. Chen, Y. Cui, J. Cho, *Adv. Energy Mater.* **2016**, 6, 1601052.
- [71] J. Zhu, M. Xiao, Y. Zhang, Z. Jin, Z. Peng, C. Liu, S. Chen, J. Ge, W. Xing, *ACS Catal.* **2016**, 6, 6335.
- [72] D. U. Lee, M. G. Park, H. W. Park, M. H. Seo, X. Wang, Z. Chen, *ChemSusChem* **2015**, 8, 3129.
- [73] M. Prabu, P. Ramakrishnan, H. Nara, T. Momma, T. Osaka, S. Shanmugam, *ACS Appl. Mater. Interfaces* **2014**, 6, 16545.
- [74] M. G. Park, D. U. Lee, M. H. Seo, Z. P. Cano, Z. Chen, *Small* **2016**, 12, 2707.
- [75] G.-P. Kim, H.-H. Sun, A. Manthiram, *Nano Energy* **2016**, 30, 130.
- [76] K. N. Jung, S. M. Hwang, M. S. Park, K. J. Kim, J. G. Kim, S. X. Dou, J. H. Kim, J. W. Lee, *Sci. Rep.* **2015**, 5, 7665.
- [77] X. Liu, M. Park, M. G. Kim, S. Gupta, X. Wang, G. Wu, J. Cho, *Nano Energy* **2016**, 20, 315.
- [78] M. Prabu, K. Ketpang, S. Shanmugam, *Nanoscale* **2014**, 6, 3173.
- [79] A. Vignesh, M. Prabu, S. Shanmugam, *ACS Appl. Mater. Interfaces* **2016**, 8, 6019.
- [80] X. Ge, F. T. Goh, B. Li, T. A. Hor, J. Zhang, P. Xiao, X. Wang, Y. Zong, Z. Liu, *Nanoscale* **2015**, 7, 9046.
- [81] M. Prabu, P. Ramakrishnan, P. Ganesan, A. Manthiram, S. Shanmugam, *Nano Energy* **2015**, 15, 92.
- [82] W. T. Hong, M. Risch, K. A. Stoerzinger, A. Grimaud, J. Suntivich, Y. Shao-Horn, *Energy Environ. Sci.* **2015**, 8, 1404.
- [83] C. Guo, Y. Zheng, J. Ran, F. Xie, M. Jaroniec, S. Z. Qiao, *Angew. Chem., Int. Ed.* **2017**, 56, 8539.
- [84] X. Liu, W. Liu, M. Ko, M. Park, M. G. Kim, P. Oh, S. Chae, S. Park, A. Casimir, G. Wu, J. Cho, *Adv. Funct. Mater.* **2015**, 25, 5799.
- [85] L. Wei, H. E. Karahan, S. Zhai, H. Liu, X. Chen, Z. Zhou, Y. Lei, Z. Liu, Y. Chen, *Adv. Mater.* **2017**, 29, 1701410.
- [86] L. Li, C. Liu, G. He, D. Fan, A. Manthiram, *Energy Environ. Sci.* **2015**, 8, 3274.
- [87] C. Ma, N. Xu, J. Qiao, S. Jian, J. Zhang, *Int. J. Hydrogen Energy* **2016**, 41, 9211.
- [88] Z. Q. Liu, H. Cheng, N. Li, T. Y. Ma, Y. Z. Su, *Adv. Mater.* **2016**, 28, 3777.
- [89] H. Cheng, M.-L. Li, C.-Y. Su, N. Li, Z.-Q. Liu, *Adv. Funct. Mater.* **2017**, 27, 1701833.
- [90] J. Fu, F. M. Hassan, C. Zhong, J. Lu, H. Liu, A. Yu, Z. Chen, *Adv. Mater.* **2017**, 29, 1702526.
- [91] M. R. Gao, Y. F. Xu, J. Jiang, S. H. Yu, *Chem. Soc. Rev.* **2013**, 42, 2986.
- [92] W. Xia, A. Mahmood, Z. Liang, R. Zou, S. Guo, *Angew. Chem., Int. Ed.* **2016**, 55, 2650.
- [93] A. Indra, P. W. Menezes, N. R. Sahraie, A. Bergmann, C. Das, M. Tallarida, D. Schmeißer, P. Strasser, M. Driess, *J. Am. Chem. Soc.* **2014**, 136, 17530.
- [94] J. Wang, L. Li, X. Chen, Y. Lu, W. Yang, *J. Mater. Chem. A* **2016**, 4, 11342.
- [95] P. Cai, J. Huang, J. Chen, Z. Wen, *Angew. Chem., Int. Ed.* **2017**, 56, 4858.
- [96] H. F. Wang, C. Tang, B. Wang, B. Q. Li, Q. Zhang, *Adv. Mater.* **2017**, 29, 1702327.
- [97] L. An, Y. Li, M. Luo, J. Yin, Y.-Q. Zhao, C. Xu, F. Cheng, Y. Yang, P. Xi, S. Guo, *Adv. Funct. Mater.* **2017**, 27, 1703779.
- [98] H.-x. Zhong, K. Li, Q. Zhang, J. Wang, F.-l. Meng, Z.-j. Wu, J.-m. Yan, X.-b. Zhang, *NPG Asia Mater.* **2016**, 8, e308.
- [99] Y. Tang, F. Jing, Z. Xu, F. Zhang, Y. Mai, D. Wu, *ACS Appl. Mater. Interfaces* **2017**, 9, 12340.
- [100] P. Ganesan, M. Prabu, J. Sanetuntikul, S. Shanmugam, *ACS Catal.* **2015**, 5, 3625.
- [101] Z. Zhang, X. Wang, G. Cui, A. Zhang, X. Zhou, H. Xu, L. Gu, *Nanoscale* **2014**, 6, 3540.
- [102] A. Sivanantham, P. Ganesan, S. Shanmugam, *Adv. Funct. Mater.* **2016**, 26, 4661.
- [103] J. Wu, S. Dou, A. Shen, X. Wang, Z. Ma, C. Ouyang, S. Wang, *J. Mater. Chem. A* **2014**, 2, 20990.
- [104] M. Wang, Y. Lai, J. Fang, F. Qin, Z. Zhang, J. Li, K. Zhang, *Catal. Sci. Technol.* **2016**, 6, 434.
- [105] X. Han, X. Wu, C. Zhong, Y. Deng, N. Zhao, W. Hu, *Nano Energy* **2017**, 31, 541.
- [106] B. Zhang, C. Xiao, S. Xie, J. Liang, X. Chen, Y. Tang, *Chem. Mater.* **2016**, 28, 6934.
- [107] Q. Zhang, Y. Wang, Y. Wang, A. M. Al-Enizi, A. A. Elzatahry, G. Zheng, *J. Mater. Chem. A* **2016**, 4, 5713.
- [108] P. Chen, K. Xu, Z. Fang, Y. Tong, J. Wu, X. Lu, X. Peng, H. Ding, C. Wu, Y. Xie, *Angew. Chem., Int. Ed.* **2015**, 54, 14710.
- [109] G. Fu, Z. Cui, Y. Chen, L. Xu, Y. Tang, J. B. Goodenough, *Nano Energy* **2017**, 39, 77.
- [110] X. Jia, Y. Zhao, G. Chen, L. Shang, R. Shi, X. Kang, G. I. Waterhouse, L. Z. Wu, C. H. Tung, T. Zhang, *Adv. Energy Mater.* **2016**, 6, 1502585.
- [111] T. Huang, S. Mao, G. Zhou, Z. Wen, X. Huang, S. Ci, J. Chen, *Nanoscale* **2014**, 6, 9608.
- [112] S. Dong, X. Chen, K. Zhang, L. Gu, L. Zhang, X. Zhou, L. Li, Z. Liu, P. Han, H. Xu, *Chem. Commun.* **2011**, 47, 11291.
- [113] Z. Cui, G. Fu, Y. Li, J. B. Goodenough, *Angew. Chem., Int. Ed.* **2017**, 56, 9901.

- [114] Q. Wang, L. Shang, R. Shi, X. Zhang, G. I. N. Waterhouse, L.-Z. Wu, C.-H. Tung, T. Zhang, *Nano Energy* **2017**, *40*, 382.
- [115] Y. Fan, S. Ida, A. Staykov, T. Akbay, H. Hagiwara, J. Matsuda, K. Kaneko, T. Ishihara, *Small* **2017**, *13*, 1700099.
- [116] Z. Cui, Y. Li, G. Fu, X. Li, J. B. Goodenough, *Adv. Mater.* **2017**, *29*, 1702385.
- [117] J. Yin, Y. Li, F. Lv, Q. Fan, Y. Q. Zhao, Q. Zhang, W. Wang, F. Cheng, P. Xi, S. Guo, *ACS Nano* **2017**, *11*, 2275.
- [118] Q. Wang, L. Shang, R. Shi, X. Zhang, Y. Zhao, G. I. N. Waterhouse, L.-Z. Wu, C.-H. Tung, T. Zhang, *Adv. Energy Mater.* **2017**, *7*, 1700467.
- [119] S. Drespe, F. Luo, R. Schmack, S. Köhl, M. Gliech, P. Strasser, *Energy Environ. Sci.* **2016**, *9*, 2020.
- [120] S. H. Ahn, A. Manthiram, *Small* **2017**, *13*, 1702068.
- [121] S. S. Shinde, C. H. Lee, A. Sami, D. H. Kim, S. U. Lee, J. H. Lee, *ACS Nano* **2017**, *11*, 347.
- [122] T. Y. Ma, J. Ran, S. Dai, M. Jaroniec, S. Z. Qiao, *Angew. Chem., Int. Ed.* **2015**, *54*, 4646.
- [123] W. Niu, Z. Li, K. Marcus, L. Zhou, Y. Li, R. Ye, K. Liang, Y. Yang, *Adv. Energy Mater.* **2018**, *8*, 1701642.
- [124] M. Yu, Z. Wang, C. Hou, Z. Wang, C. Liang, C. Zhao, Y. Tong, X. Lu, S. Yang, *Adv. Mater.* **2017**, *29*, 1602868.
- [125] S. S. Shinde, J. Y. Yu, J. W. Song, Y. H. Nam, D. H. Kim, J. H. Lee, *Nanoscale Horiz.* **2017**, *2*, 333.
- [126] H. Cheng, J. M. Chen, Q. J. Li, C. Y. Su, A. N. Chen, J. X. Zhang, Z. Q. Liu, Y. Tong, *Chem. Commun.* **2017**, *53*, 11596.
- [127] C. Guan, A. Sumboja, H. Wu, W. Ren, X. Liu, H. Zhang, Z. Liu, C. Cheng, S. J. Pennycook, J. Wang, *Adv. Mater.* **2017**, *29*, 1704117.
- [128] M. Wang, S. Liu, N. Xu, T. Qian, Ch. Yan, *Adv. Sustainable Syst.* **2017**, *1*, 1700085.
- [129] C. Lin, S. Shinde, Y. Wang, Y. Sun, S. Chen, H. Zhang, X. Li, J. H. Lee, *Sustainable Energy Fuels* **2017**, *1*, 1909.
- [130] A. Sumboja, M. Lübke, Y. Wang, T. An, Y. Zong, Z. Liu, *Adv. Energy Mater.* **2017**, *7*, 1700927.
- [131] J. F. Parker, C. N. Chervin, E. S. Nelson, D. R. Rolison, J. W. Long, *Energy Environ. Sci.* **2014**, *7*, 1117.
- [132] X. Chen, B. Liu, C. Zhong, Z. Liu, J. Liu, L. Ma, Y. Deng, X. Han, T. Wu, W. Hu, J. Lu, *Adv. Energy Mater.* **2017**, *7*, 1700779.
- [133] F. Meng, H. Zhong, D. Bao, J. Yan, X. Zhang, *J. Am. Chem. Soc.* **2016**, *138*, 10226.
- [134] X. Cai, B. Y. Xia, J. Franklin, B. Li, X. Wang, Z. Wang, L. Chen, J. Lin, L. Lai, Z. Shen, *J. Mater. Chem. A* **2017**, *5*, 2488.
- [135] Q. Liu, Y. Wang, L. Dai, J. Yao, *Adv. Mater.* **2016**, *28*, 3000.
- [136] S. Zeng, H. Chen, H. Wang, X. Tong, M. Chen, J. Di, Q. Li, *Small* **2017**, *13*, 1700518.
- [137] Y. Xu, Y. Zhang, Z. Guo, J. Ren, Y. Wang, H. Peng, *Angew. Chem., Int. Ed.* **2015**, *54*, 15390.
- [138] B. Li, X. Ge, F. W. Goh, T. S. Hor, D. Geng, G. Du, Z. Liu, J. Zhang, X. Liu, Y. Zong, *Nanoscale* **2015**, *7*, 1830.
- [139] P. Tan, B. Chen, H. Xu, H. Zhang, W. Cai, M. Ni, M. Liu, Z. Shao, *Energy Environ. Sci.* **2017**, *10*, 2056.
- [140] S. Chen, J. Duan, P. Bian, Y. Tang, R. Zheng, S.-Z. Qiao, *Adv. Energy Mater.* **2015**, *5*, 1500936.
- [141] L. Li, A. Manthiram, *Adv. Energy Mater.* **2016**, *6*, 1502054.
- [142] D. U. Lee, J.-Y. Choi, K. Feng, H. W. Park, Z. Chen, *Adv. Energy Mater.* **2014**, *4*, 1301389.
- [143] J. Fu, F. M. Hassan, J. Li, D. U. Lee, A. R. Ghannoum, G. Lui, M. A. Hoque, Z. Chen, *Adv. Mater.* **2016**, *28*, 6421.
- [144] I. S. Amiin, X. Liu, Z. Pu, W. Li, Q. Li, J. Zhang, H. Tang, H. Zhang, S. Mu, *Adv. Funct. Mater.* **2018**, *28*, 1704638.
- [145] I. S. Amiin, Z. Pu, X. Liu, K. A. Owusu, H. G. R. Monestel, F. O. Boakye, H. Zhang, S. Mu, *Adv. Funct. Mater.* **2017**, *27*, 1702300.
- [146] T. Wang, Z. Kou, S. Mu, J. Liu, D. He, I. S. Amiin, W. Meng, K. Zhou, Z. Luo, S. Chaemchuen, F. Verpoort, *Adv. Funct. Mater.* **2018**, *28*, 1705048.